

UNIVERSITY OF SOUTHAMPTON  
FACULTY OF MATHEMATICAL SCIENCES



**Mathematics for Audiophiles**  
Approximating the Sound Pressure Field in Small  
Rooms

Evan Turnill

A project report submitted for the award of B.Sc Mathematics

Supervised by Ian Hawke

May 2016

## Acknowledgements

I thank Ian Hawke for his support during this project. His extensive knowledge of numerical methods was an invaluable resource and his ability to see errors in my MATLAB code was essential to my endeavours. I also thank Chris Walls, who suggested to me that I might find the acoustics of small rooms an interesting subject matter for this project. I am also grateful to him for allowing me to use his equipment (and his lounge) to provide a set of real data points to compare with my models.

## **Abstract:**

This project provides a detailed mathematical analysis of how low frequency sound waves propagate and interact in the relatively small rooms that are commonly used for home cinemas or music studios. In particular, the causes of resonant frequencies and their adverse effect on the experience of a listener in the room are explored. The time dependent scalar wave equation is derived to describe how the sound pressure field varies with time and the time independent Helmholtz equation is derived in order to describe the standing waves that relate to resonant frequencies. Solutions to the Helmholtz equation are then found and used to form a mode summation method for approximating the sound field in a small rectangular room with a single source. A further approximation is developed using a finite difference representation of the wave equation. Both methods are implemented using MATLAB and compared against actual data measured in a real room. The results of these tests show that the approximations produced fail to exactly represent the sound field in the room, but do give an indication of the range of frequencies where particular problems will be experienced. It is concluded that the discrepancies between the models and data are likely to have been caused by various approximations made in their derivation.

## Contents

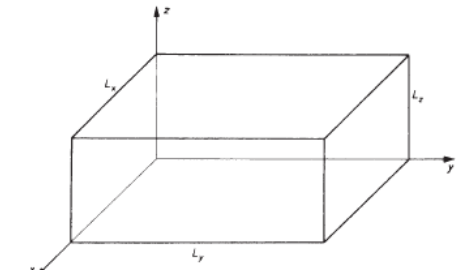
Acknowledgements .....	1
Abstract: .....	2
1. Introduction .....	5
2. The nature of sound.....	6
2.1. Sound propagation in free space .....	6
2.2. Enclosed spaces and acoustic resonances .....	7
3. Derivation of the Wave equation.....	9
3.1. Eulerian and Lagrangian coordinates.....	9
3.2. Conservation of mass.....	10
3.3. Conservation of linear momentum.....	11
3.4. Assumption of small amplitude.....	13
3.5. Equation of state.....	13
4. Derivation of the Helmholtz equation.....	14
5. Resonances in rooms.....	15
5.1. Solutions of the Helmholtz equation.....	15
5.2. Effect of the room modes .....	17
5.3. Modal density.....	18
5.4. Classes of room mode.....	19
5.5. Orthogonality and completeness of eigenfunctions .....	19
5.6. Energy of modes .....	20
6. Mode summation method .....	21
6.1. MATLAB implementation of modal summation method.....	23
7. Reflectance, absorption and impedance .....	23
8. Finite difference time domain method (FDTD).....	25
8.1. Finite differences.....	25
8.2. Discretisation .....	27
8.3. Boundary conditions.....	28
8.3.1. Boundary points that are not on an edge or a corner .....	28
8.3.2. Boundary points that are on an edge .....	29
8.3.3. Boundary points on a corner .....	30
8.4. Conversion to frequency domain .....	30
8.5. MATLAB implementation of FDTD method .....	30

9.	Actual measurement.....	31
9.1.	The room.....	31
9.2.	The measurement method .....	31
9.3.	The speaker and microphone positions .....	31
9.4.	Calculation of absorption coefficients of the walls for use in implementations .....	33
10.	Results .....	34
10.1.	Comparison of the models with actual measurements .....	34
10.2.	Differences between the two models.....	34
11.	Conclusion.....	38
	References .....	40
	Appendix.....	43

## 1. Introduction

The aim of this project is to investigate the way low frequency sound behaves in small rectangular rooms. This is motivated by the desire to obtain a high quality listening experience in rooms such as home cinemas and small music or film editing suites. Although most rooms are not exactly rectangular, many are approximately this shape. Therefore, for the purposes of this project, we will limit ourselves to this case (see figure 1). For simplicity, we will also limit ourselves to a single sound source, which will represent a single speaker in the room. The methods discussed below could easily be extended to a room with multiple sources.

Figure 1 Rectangular room  
Image: (Kuttruff, 2009, p. 72)



The rectangular room with dimensions  $L_x$  by  $L_y$  by  $L_z$ , which will be the basis of the mathematical models in this report.

If a sound source produces waves of a single frequency, the sound wave can be represented as a pure sine wave. When these waves reflect from the walls and ceilings they will combine to form 'standing waves'. At some points in the room the amplitude of these waves will be zero (nodes) and at some there will be pressure difference maximums (anti-nodes). Therefore, if the speaker produces wave of a single frequency, there may be positions in the room when a listener would not, in theory, be able to tell the speaker was producing any sound.

In practice, most sound is made up of a variety of frequencies. These more complex sound waves can be considered to be a sum of many pure sine waves. Each of the components of the complex sound wave will generate different standing waves in the room. At a given point in the room, the components of waves with certain frequencies may be near a node whilst others will be near an anti-node. For this reason, a listener may hear certain frequencies louder than others, even if the speaker originally generated a wave where the output level of each frequency was identical.

In this project, we will look in detail at the cause of this phenomenon and will show why it is particularly noticeable when low frequency sounds are played in small rooms. To do this, we will derive from first principles both a time dependent equation to describe the pressure field in the room (the wave equation) and a time independent equation which describes the standing waves in the room (the Helmholtz equation).

We will also look at two methods for approximating the pressure field in a small room with a single source and will implement these methods in MATLAB (Mathworks, 2015). Primarily, this will be done as a way of demonstrating the particular problems of low frequency sounds in small rooms. However, we will also evaluate whether these could be used as a 'rough and ready' way of demonstrating the deficiencies of particular listening rooms and of specific locations of speaker and listener within them. To do this, actual measurements have been taken of a real room to compare with those approximated using the two MATLAB implementations.

The results of these tests show that the approximations produced fail to exactly represent the sound field in the room, but do give an indication of the range of frequencies where particular problems will be experienced. We conclude that further refinement of the methods or an implementation of a more sophisticated model (such as Finite Element Method ("FEM") or Boundary Element Method ("BEM")) should be investigated.

## 2. The nature of sound

It is useful to first consider in a qualitative way how sound behaves, both in free space and when in an enclosed space.

### 2.1. Sound propagation in free space

A speaker generates sound by using an electric current to oscillate a thin cone at varying speeds. As the cone moves back and forth, the air particles in the surrounding area are pushed together (compressed) and pulled apart (rarefied). This causes the density and air pressure to vary. The difference between the static air pressure in a room and the instantaneous pressure caused by these variations is called sound pressure. The propagation of sound pressure changes through space and time is known as a sound wave (Kuttruff, 2009, p.7).

The sound wave moves through air at a speed determined by, among other things, the static pressure and density of the air as well as the frequency and amplitude of the sound wave travelling through it. This means humidity and temperature also affect the speed of sound. In this project it has been assumed that the speed of sound is 343 metres per second and that this is independent of frequency and amplitude. This is based on a room temperature of 20 degrees and assumes that air is stationary (no air conditioning or wind) (Kuttruff, 2009, p.7).

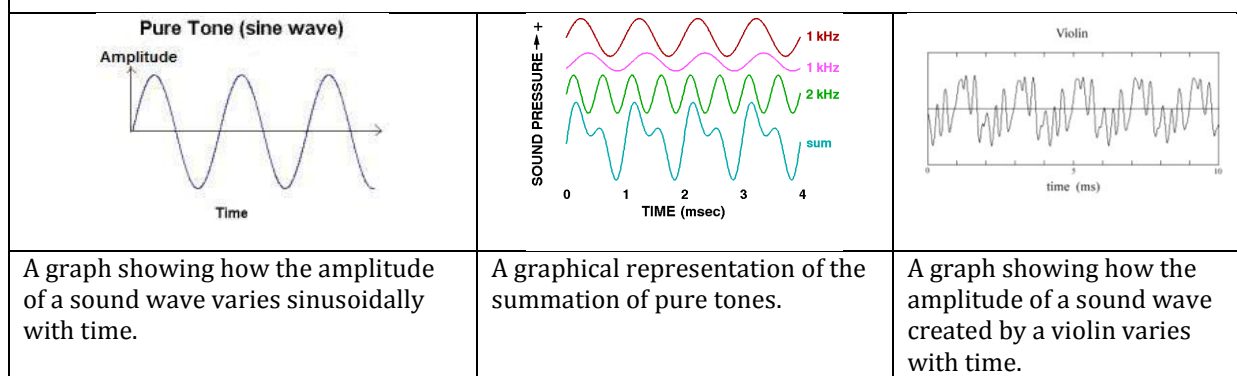
As the wave propagates through the air, energy is lost causing the pressure variations to decay. This process is known as attenuation or absorption. In air, over small distances, this energy loss is very small. Given that this project is interested in small rooms, attenuation through the air will be treated as negligible and will not be taken into account.

In a lossless medium, as we are treating air to be, the variations in sound pressure and particle velocity are periodic. This means, for example, that at a fixed point  $\mathbf{x}(x, y, z)$ , the amplitude  $p$  of the wave will vary in a given period  $T$  identically to the next period of the same length. Equivalently,  $p(\mathbf{x}) = p(\mathbf{x} + nT)$ , where  $n \in \mathbb{Z}$ . A wave of a pure tone could therefore be described with a sine or cosine function (see figure 2).

Real sound waves are composed of many different frequencies. However, these waves can be represented by a sum of other sine or cosine waves (see figure 2). Although this feels intuitively true, a more detailed mathematical proof can be found in any text book on Fourier analysis (e.g. (Stein and Shakarchi, 2003)). The complexities of real sound waves, such as those created by a violin, can also be seen at figure 2.

Figure 2

Images: (University of Salford, no date), (Indiana University, no date), (Harmonics in a violin tone, no date)



If we take the example of a wave moving in the  $x$  direction in an unbounded region, this can be described as follows:  $p(x, t) = A \cos(\omega t - kx)$ , where  $A$  and  $k$  are arbitrary constants and  $\omega$  is a quantity known as the angular frequency. Angular frequency is the rate of change of the argument of the cosine function measured in Radians per second. Fields for which the time variation is sinusoidal are also known as time-harmonic fields. Therefore waves such as we have just described are known as time-harmonic waves.

We can relate the angular frequency to other important characteristics of a wave. We let  $T$  equal the period of the wave. This is time taken for a complete cycle of the wave measured in seconds. We let  $\lambda$  equal the wavelength. This is spatial distance over which a complete cycle is completed and is measured in metres. We let  $f$  equal the ordinary frequency of the wave. This indicates the number of cycles per second and is measured in Hertz. Finally, we let  $k$  be the wave number. This represents the number of radians per unit distance and has units of 1/meters. These quantities are related as follows (Kuttruff, 2009, p.10):

$$f = \frac{1}{T} ; \quad T = \frac{2\pi}{\omega} ; \quad \lambda = \frac{2\pi}{k} = \frac{2\pi c}{\omega} ; \quad \omega = kc = 2\pi f ; \quad k = \frac{2\pi}{\lambda}. \quad (1)$$

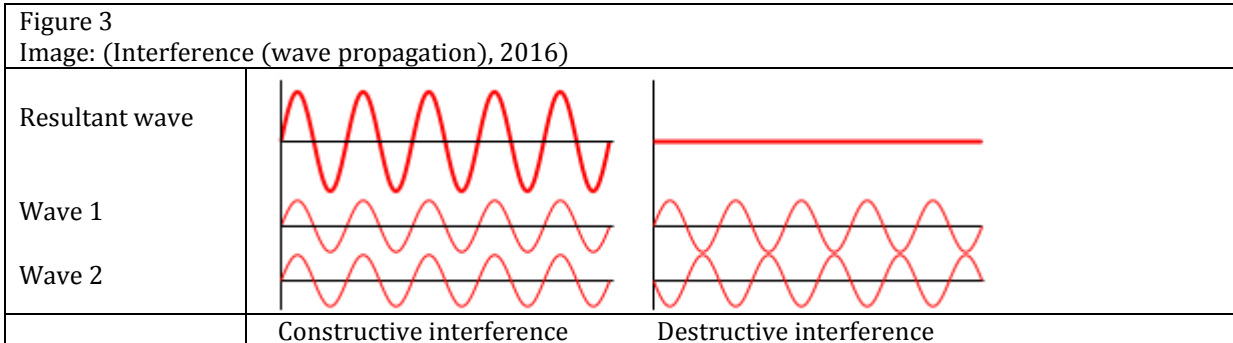
## 2.2. Enclosed spaces and acoustic resonances

We have considered how sound propagates in free space. However, this project involves soundwaves in a room so we also need to consider how sound behaves in an enclosed space.

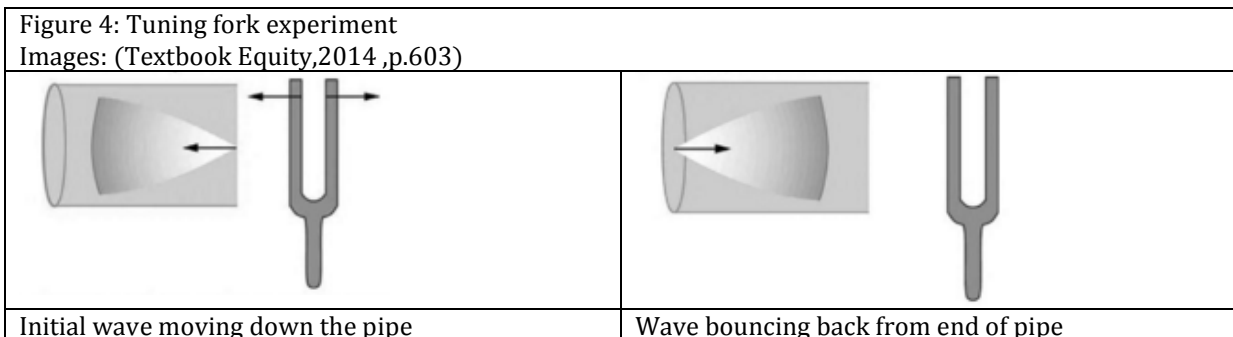
If a sound wave meets an object which is denser than air, for example a wall, the energy in the wave travelling in that direction will be subject to absorption. Further, the wave may be reflected or refracted. The degree of absorption, reflection and refraction will depend on the angle of incidence the wave makes with the surface of the wall, the material the wall is made from and the shape of the wall. This is discussed in more detail later in this report in section 7.

If waves are reflected in an enclosed space, the reflected waves will interact. This interaction means that the size and shape of that space can have a significant effect on the amplitude of the wave at each point in the room making certain frequencies appear to be louder than others.

To understand the mechanism that causes this, we first must consider the concepts of constructive and destructive interference. Two identical waves that meet which are exactly in phase will constructively interfere with each other thereby doubling the amplitude. Two waves that are out of phase by an odd multiple of  $\pi$  will destructively interfere with each other effectively cancelling each other out (see figure 3).

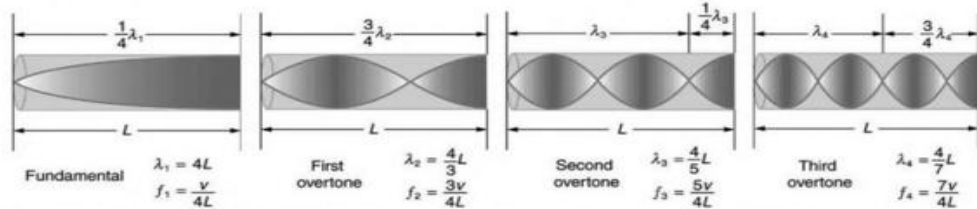


A simple experiment, involving a tuning fork and a tube, can demonstrate how interference occurs in enclosed spaces. The tube is open at the end near the tuning fork and closed at the other. Sound waves therefore travel down the tube and are reflected back from the closed end (see figure 4). If the tuning fork produces soundwaves with certain particular frequencies, the air in the pipe will resonate loudly. These frequencies are known as resonant frequencies. At other frequencies the pipe will resonate very little.



If the frequency is chosen such that the pipe is exactly a quarter of the wavelength of the sound wave, then the wave will return to the fork half a cycle later. This constructively interferes with the wave being created by the fork, doubling its amplitude. This is a resonant frequency. Figure 5 shows the 'standing wave' created when this happens. The points where the amplitude does not vary are known as nodes. The points where the amplitude variation is maximised are known as anti-nodes. The resonant frequency with the longest wavelength is known as the fundamental frequency. If the frequency of the tuning fork is at odd multiples of the fundamental frequency, the tube of air will also resonate. These resonances are known as overtones. In systems where the wave is fixed at one end (as here) only odd multiples will resonate. If a system is fixed at both ends then all integer multiples of the fundamental frequency will be overtones.

Figure 5  
Image: (Textbook Equity, 2014 ,p.604)



Standing waves in a pipe generated by particular resonant frequencies.

In a room, just as in the test tube, there are certain frequencies which will produce standing waves with nodes and anti-nodes. Again, at an anti-node, far greater excitation of the air will occur. These resonant frequencies are also known as 'modal frequencies'. Just as the resonant frequencies of the pipe were determined by its length, we will see that the modal frequencies of a room are determined by the dimensions of the room.

The modal frequencies of a room are of importance to the quality of the listening experience of those in it. A person seeking to listen to music in a room desires to hear all the frequencies as close as possible to the levels at which they were recorded. However, if one frequency is particularly excited because it is close to a resonant frequency, the amplitude of this frequency will appear higher than it should.

To provide a mathematical explanation of this, we now need to derive an equation to describe the propagation of sound waves in a three dimensional room. This equation is known as the scalar wave equation and is time dependent. However, given that sound at frequencies other than the modal frequencies will not greatly excite the room, the properties that will be most important in defining the acoustic characteristics of the room will be the standing waves generated by the modal frequencies. We will therefore also want to derive a time independent version of the wave equation known as the Helmholtz equation.

### 3. Derivation of the Wave equation

#### 3.1. Eulerian and Lagrangian coordinates

Before embarking on the derivation of the wave equation it is essential that we consider how we will describe properties in an air flow. When we describe the propagation of a sound wave, it will be important whether the medium itself (i.e. the air in the room) is stationary or moving. If the air is moving (caused by wind or other disturbances) this may affect how the wave propagates. This can be taken into account by the use of two different coordinate systems to describe the flow of air, namely the Eulerian and Lagrangian systems. MacArthur (2015, pp.11-12) provides the following definition and accompanying analogies of both.

The Eulerian system measures properties at a fixed point  $\mathbf{x} = (x, y, z)$ . A helpful analogy is to think of a man stood in a river measuring the properties of the flow as it moves past him. The Eulerian time derivative, holding  $\mathbf{x}$  fixed, is written  $\frac{\partial}{\partial t} \equiv \frac{\partial}{\partial t} \Big|_{\mathbf{x}}$ .

The Lagrangian system labels air ‘particles’ and allows coordinates  $\mathbf{X} = (X, Y, Z)$  to move with the air flow, measuring properties as material particles move through different points in space. An appropriate analogy for this is to think of a man in a boat measuring the properties of the flow as he travels down the river.

The Lagrangian or material time derivative, holding  $\mathbf{X}$  fixed, is written  $\frac{d}{dt} \equiv \frac{\partial}{\partial t} \Big|_{\mathbf{X}}$ . If we let  $\varphi(\mathbf{x}, t)$  be a differentiable scalar function, the two systems can be related by use of the chain rule as follows:

$$\frac{d\varphi}{dt} = \frac{\partial}{\partial t} \Big|_{\mathbf{X}} \varphi(\mathbf{x}(\mathbf{X}, t), t) \quad (2)$$

$$\Rightarrow \frac{d\varphi}{dt} = \frac{\partial \varphi}{\partial x} \frac{\partial x}{\partial t} \Big|_{\mathbf{X}} + \frac{\partial \varphi}{\partial y} \frac{\partial y}{\partial t} \Big|_{\mathbf{X}} + \frac{\partial \varphi}{\partial z} \frac{\partial z}{\partial t} \Big|_{\mathbf{X}} + \frac{\partial \varphi}{\partial t} \quad (3)$$

$$\Rightarrow \frac{d\varphi}{dt} = \frac{\partial \varphi}{\partial x} \frac{dx}{dt} + \frac{\partial \varphi}{\partial y} \frac{dy}{dt} + \frac{\partial \varphi}{\partial z} \frac{dz}{dt} + \frac{\partial \varphi}{\partial t} \quad (4)$$

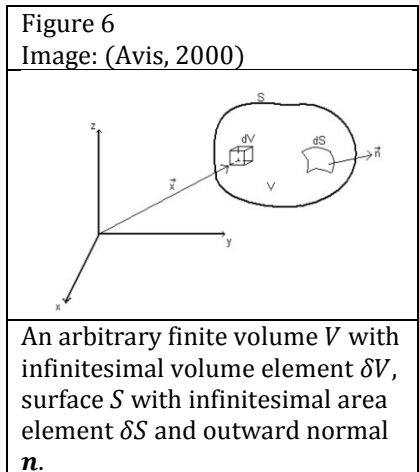
$$\Rightarrow \frac{d\varphi}{dt} = \frac{\partial \varphi}{\partial x} v_x + \frac{\partial \varphi}{\partial y} v_y + \frac{\partial \varphi}{\partial z} v_z + \frac{\partial \varphi}{\partial t} \quad (5)$$

$$\frac{d\varphi}{dt} = \frac{\partial \varphi}{\partial t} + (\mathbf{v} \cdot \nabla) \varphi \quad (6)$$

We are now ready to derive an equation that provides a description of a sound wave. This derivation is founded on two principles of conservation: conservation of mass and conservation of momentum. We shall look at each in turn.

### 3.2. Conservation of mass

We consider an arbitrary volume  $V$  of air, with a surface area  $S$ , with outward normal unit vector  $\mathbf{n}$  (see figure 6). We assume  $V$  is stationary. We let  $\rho(x, y, z, t)$  be the density of the air ( $kg/m^3$ ) and  $Q(x, y, z, t)$  be a source function injecting air into  $V$  at a rate of  $\rho Q(x, y, z, t)$  per unit volume.  $Q$  could represent a speaker producing air flow inside a room. At time  $t$ , the mass of air inside  $V$  is equal to  $\int_V \rho dV$ .



We can therefore write the rate of change of mass as

$$\frac{d}{dt} \int_V \rho dV = \int_V Q \rho dV - \int_S (\rho \mathbf{v}) \cdot \mathbf{n} dS, \quad (7)$$

where  $\mathbf{v}(x, y, z, t)$  is the velocity of each volume element  $\delta V$  and  $\frac{d}{dt}$  is equal to the material time derivative. From the definition of the total time derivative (6), we can see that

$$\frac{d\rho}{dt} = \frac{\partial\rho}{\partial t} + (\rho \cdot \nabla)\rho. \quad (8)$$

Given  $V$  is stationary, and for the reasons discussed in section 3.1 above, we can also write the rate of change of mass as

$$\frac{d}{dt} \int_V \rho dV = \int_V \frac{d\rho}{dt} dV = \int_V \frac{\partial\rho}{\partial t} + (\rho \cdot \nabla)\rho dV = \int_V \frac{\partial\rho}{\partial t} dV. \quad (9)$$

By the divergence theorem (Riley, Hobson and Bence, 2006, p.401), we can rewrite the surface integral in (7) above as

$$\int_S (\rho \mathbf{v}) \cdot \mathbf{n} dV = \int_V \nabla \cdot (\rho \mathbf{v}) dV. \quad (10)$$

This allows us to rewrite the rate of change of mass equation (7) in terms of three volume integrals:

$$\int_V \frac{\partial\rho}{\partial t} dV = \int_V Q \rho dV - \int_V \nabla \cdot (\rho \mathbf{v}) dV. \quad (11)$$

As this equation holds for any  $V$ , This implies that

$$\frac{\partial\rho}{\partial t} + \nabla \cdot (\rho \mathbf{v}) = Q. \quad (12)$$

This is known as the conservation of mass equation or the continuity equation.

### 3.3. Conservation of linear momentum

We again consider the same volume  $V$  as defined above. The momentum of the Volume  $V$  at an instant  $t$  is given by the sum of the mass of each volume unit  $\delta V$  multiplied by its velocity  $\mathbf{v}$ . By Newton's second law, we know that the rate of change of momentum of an object is equal to the sum of the forces acting upon it.

We therefore have that

$$\frac{d}{dt} \int_V \rho \mathbf{v} dV = \int_V \rho \mathbf{b} dV + \int_S \mathbf{t} dS , \quad (13)$$

where  $\int_V \rho \mathbf{b} dV$  is equal to the body forces acting on the volume and  $\int_S \mathbf{t} dS$  is equal to the surface forces acting on the volume due to the air flow.

The body forces for our purposes include gravity, where  $\mathbf{b} = -g\hat{\mathbf{k}}$ . However, the effect of this body force will be negligible compared to the surface forces and we will disregard it.

The surface forces are composed of both the tangential friction forces that are applied to a particle moving through the air and the normal forces which act upon it due to pressure. The stress vector  $\mathbf{t}$  can be written, using index summation notation, as  $\mathbf{t} = \sigma_{ij}n_j$ , where  $\sigma_{ij}$  is a tensor that gives the force per unit area in the  $x_i$  direction acting on a surface element whose normal is in the  $x_j$  direction (Ockendon & Ockendon, 1995, p.4).

We now wish to change the surface integral of  $\mathbf{t}$  into a volume integral. We again use the divergence theorem to find that

$$\int_S \mathbf{t} dS = \int_S \sigma_{ij}n_j dS = \int_V \nabla \cdot \boldsymbol{\sigma} dV . \quad (14)$$

The stress tensor can be expressed as the combination of an isotropic part  $-p\delta_{ij}$  (which relates to the pressure element) and a deviatoric part  $d_{ij}$  (that relates to the viscous forces) so that  $\sigma_{ij} = -p\delta_{ij} + d_{ij}$  (Macarthur, 2015, p.16). The tangential forces that act on an air particle as it moves through air are negligible, so we disregard these forces. Setting  $d_{ij}$  to zero and taking the divergence of both sides implies that  $\nabla \cdot \boldsymbol{\sigma} = -\nabla p$ .

Rearranging the LHS of the rate of change of linear momentum equation (13) implies that

$$\frac{d}{dt} \int_V \rho \mathbf{v} dV = \int_V \frac{d(\rho \mathbf{v})}{dt} dV = \int_V \rho \frac{d\mathbf{v}}{dt} dV . \quad (15)$$

The linear momentum equation (13) can therefore be rewritten as

$$\int_V \rho \frac{d\mathbf{v}}{dt} dV = \int_V -\nabla p dV . \quad (16)$$

Again, as  $V$  is arbitrary, this implies that

$$\rho \frac{d\mathbf{v}}{dt} + \nabla p = \mathbf{0} . \quad (17)$$

Taking each component of  $\mathbf{v}$  in turn and applying the definition of the total derivative (6), we see that:

$$\frac{d\mathbf{v}}{dt} = \frac{\partial \mathbf{v}}{\partial t} + \frac{\partial \mathbf{v}}{\partial x} \frac{\partial x}{\partial t} + \frac{\partial \mathbf{v}}{\partial y} \frac{\partial y}{\partial t} + \frac{\partial \mathbf{v}}{\partial z} \frac{\partial z}{\partial t} = \frac{\partial \mathbf{v}}{\partial t} + (\mathbf{v} \cdot \nabla) \mathbf{v}. \quad (18)$$

We can therefore rewrite (17) in the following form:

$$\rho \left[ \frac{\partial \mathbf{v}}{\partial t} + (\mathbf{v} \cdot \nabla) \mathbf{v} \right] + \nabla p = 0, \quad (19)$$

which is known as Euler's equation.

### 3.4. Assumption of small amplitude

Another assumption we choose to make is that any change in amplitude is small. In this way we are will be able to linearise any non-linear equations. We therefore assume that:  $\rho = \rho_0 + \tilde{\rho}$   $p = p_0 + \tilde{p}$ , where  $\tilde{\rho}$  and  $\tilde{p}$  are small perturbations and  $\rho_0$  and  $p_0$  are the static state.

Substituting these values into the continuity equation (12) and Euler's equation (19) implies that

$$\frac{\partial \tilde{p}}{\partial t} + (\mathbf{v} \cdot \nabla) \tilde{p} + \rho_0 c^2 \nabla \cdot \mathbf{v} = Q \quad (20)$$

and

$$\rho_0 \left[ \frac{\partial \mathbf{v}}{\partial t} + (\mathbf{v} \cdot \nabla) \mathbf{v} \right] + \nabla \tilde{p} = 0. \quad (21)$$

### 3.5. Equation of state

Even with the above assumptions we have too few equations to solve for the number of unknowns. We therefore need a further relationship between two of the unknowns. This further relationship is known as the equation of state and relates the pressure to the density. To find this relationship we make the assumption that air is an ideal gas and that sound waves compress the air in an adiabatic way (Acoustic Theory, 2015). Making these assumptions means the following equations of state can be relied upon:

$$\frac{dp}{d\rho} = \frac{\gamma p}{\rho}; c^2 = \frac{\gamma p}{\rho}, \quad (22)$$

where  $c$  is the wave speed and  $\gamma$  is the ratio of the specific heat of air at constant pressure to the specific heat of air at constant volume. The derivation of these equations can be found at (Morse, 1948, p. 220) and (Introduction to Physical Chemistry, no date). Again, assuming small disturbances, this implies:

$$\frac{dp}{d\rho} \approx \frac{\tilde{p}}{\tilde{\rho}}; \frac{p}{\rho} \approx \frac{p_0}{\rho_0}; c^2 \approx c_0^2 = \frac{\gamma p_0}{\rho_0} \quad (23)$$

where  $c_0$  is the speed of sound in air static air which we assume approximates the wave speed in the disturbed field. Therefore we can see  $\frac{\tilde{p}}{\tilde{\rho}} = c_0^2$ .

Differentiating with respect to  $t$  implies that

$$\frac{\partial \tilde{p}}{\partial t} = c_0^2 \frac{\partial \tilde{p}}{\partial t} \quad (24)$$

Substituting this into the perturbed continuity of mass (20) and Euler's equations (21) and disregarding any products of the perturbations (i.e. linearising) implies that

$$\frac{\partial \tilde{p}}{\partial t} + \rho_0 c_0^2 \nabla \cdot \mathbf{v} = Q \quad (25)$$

$$\rho_0 \frac{\partial \mathbf{v}}{\partial t} + \nabla \tilde{p} = 0 \quad (26)$$

Differentiating the first of these equations(25) with respect to  $t$  and taking the divergence of the second (26) gives that

$$\frac{\partial^2 \tilde{p}}{\partial t^2} + \rho_0 c_0^2 \frac{\partial}{\partial t} (\nabla \cdot \mathbf{v}) = \frac{\partial Q}{\partial t} \quad (27)$$

$$\rho_0 \frac{\partial}{\partial t} (\nabla \cdot \mathbf{v}) + \nabla^2 \tilde{p} = 0 \quad (28)$$

Dropping the tildas and combining these two equations gives the scalar wave equation:

$$\frac{\partial^2 p}{\partial t^2} - c^2 \nabla^2 p = \frac{\partial Q}{\partial t} . \quad (29)$$

If there is no source, then the RHS of the equation will be equal to zero. This is known as the homogeneous wave equation. If there is a source such that the RHS is non-zero, then it is known as the inhomogeneous wave equation

#### 4. Derivation of the Helmholtz equation

As stated above, the Helmholtz equation, a time independent version of the wave equation, will allow us to find the standing waves in the room which correspond to the modal frequencies.

This derivation is based on that of Runborg (2012, p.1). The starting point is the scalar wave equation we have already derived, namely

$$\frac{\partial^2 p}{\partial t^2} - c^2 \nabla^2 p = \frac{\partial Q}{\partial t} . \quad (30)$$

As discussed above in section 2, a plane wave travelling in a lossless medium in the  $x$ -direction with a specific angular frequency  $\omega$  can be described by the following equation:  $p(x, t) = \hat{p}(x) \cos(\omega t - kx)$ , where  $\hat{p}(x)$  represents the maximum amplitude of the wave.

It will be useful to describe these waves using complex notation. Using the fact that  $e^{ix} = \cos x + i \sin x$  (Euler's identity), we can write:  $p(x, t) = \operatorname{Re} \{ \hat{p}(x) e^{i(\omega t - kx)} \}$  where  $\operatorname{Re}$  denotes taking of the real part. We shall now omit the  $\operatorname{Re}$  from our notation, but must remember that this is implied.

In three dimensions, we are therefore looking for solutions to the wave equation with the form

$$p(t, x, y, z) = \hat{p}(x, y, z)e^{-i\omega t} . \quad (31)$$

We also assume that the source generates waves of this form

$$Q(t, x, y, z) = q(x, y, z)e^{-i\omega t} . \quad (32)$$

Substituting these two equations into the inhomogeneous wave equation (30) implies that

$$-\omega^2 \hat{p}(x, y, z)e^{-i\omega t} = c(x, y, z)^2 \nabla^2 \hat{p}(x, y, z)e^{-i\omega t} + i\omega q(x, y, z)e^{-i\omega t} . \quad (33)$$

Finally, rearranging this, dividing by  $e^{-i\omega t}$  and dropping the hats implies that

$$\nabla^2 p + \frac{\omega^2}{c^2} p = -i\omega q . \quad (34)$$

This is the inhomogeneous version of the Helmholtz wave equation. If there were no source term, the RHS of the equation would be equal to zero and we would have the homogeneous Helmholtz equation. Solutions to the Helmholtz equation represent the spatial distribution of the amplitudes of the resonant frequencies.

## 5. Resonances in rooms

Having derived the Helmholtz equation, we now have the tools required to find the standing waves in a room. For simplicity, we shall at first assume that the room has rigid walls, so that the wave is reflected back into the room without loss. The effect of non-rigid walls will be considered further in section 6 and 7 below.

The standing waves will be provided by the solutions of the inhomogeneous Helmholtz equation. The following method for finding the solutions to the Helmholtz equation (sections 5 and 6 of this report) follow closely the method used by Kutruff (2009, pp.1-71). However, his work is largely based on the work of Morse (1948, pp. 389-418). In fact, most modern texts on acoustics rely heavily upon Morse's excellent works from the 1940s to the 1970s, which set out in great detail the foundations of the subject.

### 5.1. Solutions of the Helmholtz equation

The source free or homogenous Helmholtz equation can be written as

$$\nabla^2 p + k^2 p = \frac{\partial^2 p}{\partial x^2} + \frac{\partial^2 p}{\partial y^2} + \frac{\partial^2 p}{\partial z^2} + k^2 p = 0 , \quad (35)$$

where  $k = \frac{\omega}{c}$ .

The solution to this equation can be rewritten in a separated form as

$$p(x, y, z) = p_x(x)p_y(y)p_z(z) . \quad (36)$$

where  $p_x, p_y$  and  $p_z$  are the components of  $p$  in the  $x, y$  and  $z$  directions respectively.

Substituting this into the Helmholtz equation gives the following three equations:

$$\frac{\partial^2 p_x}{\partial x^2} + k_x p_x = 0 ; \frac{\partial^2 p_y}{\partial y^2} + k_y p_y = 0 ; \frac{\partial^2 p_z}{\partial z^2} + k_z p_z = 0 , \quad (37)$$

where the constants  $k_x$ ,  $k_y$  and  $k_z$  are related by:

$$k^2 = k_x^2 + k_y^2 + k_z^2 . \quad (38)$$

The assumption that the walls of the room are rigid implies that at the boundary, the particle velocity is zero. This implies that at the boundaries

$$\frac{\partial p_x}{\partial x} = \frac{\partial p_y}{\partial y} = \frac{\partial p_z}{\partial z} = 0 . \quad (39)$$

These equations are second order homogeneous partial differential equations. It can easily be shown that the general solution of the  $x$  equation is

$$p_x(x) = A_1 \cos(k_x x) + B_1 \sin(k_x x) , \quad (40)$$

where  $A_1$  and  $B_1$  are constants.

Differentiating this with respect to  $x$  gives:

$$\frac{\partial p_x}{\partial x}(x) = -k_x A_1 \sin(k_x x) + g_x B_1 \cos(k_x x) \quad (41)$$

As  $\frac{\partial p_x}{\partial x} = 0$  at  $x = 0$ , we can see  $B_1 = 0$ . As  $\frac{\partial p_x}{\partial x} = 0$  at  $x = L_x$ , we can see  $A_1 = 0$  or  $k_x = \frac{n_x \pi}{L_x}$ .  $A_1 = 0$  is not compatible with any solution other than the trivial case. Therefore the only allowed solutions are  $k_x = \frac{n_x \pi}{L_x}$ . The other equations will have solutions of the same form.

Substituting these solutions into the formula for the wave number (38) gives:

$$k_{n_x n_y n_z} = \left[ \left( \frac{n_x \pi}{L_x} \right)^2 + \left( \frac{n_y \pi}{L_y} \right)^2 + \left( \frac{n_z \pi}{L_z} \right)^2 \right]^{\frac{1}{2}} , \quad (42)$$

which are known as the eigenvalues of the wave and Helmholtz equations. Substituting the values of  $k_x$ ,  $k_y$  and  $k_z$  into each of the general solutions for the  $x$ ,  $y$  and  $z$  directions (40) and then into the equation of the solution in separated form given at (36) and combining the constants gives that

$$p_{n_x n_y n_z} = C \cos\left(\frac{n_x \pi x}{L_x}\right) \cos\left(\frac{n_y \pi y}{L_y}\right) \cos\left(\frac{n_z \pi z}{L_z}\right) , \quad (43)$$

where  $C$  is an arbitrary constant that represents the maximum amplitude of the sound pressure.

$p_{n_x n_y n_z}$  represents what are known as the eigenfunctions of the wave and Helmholtz equations. These eigenfunctions describe the three dimensional standing waves we have been looking for. These are also referred to as normal or room modes.

Wherever  $\cos\left(\frac{n_x \pi x}{L_x}\right)$  or  $\cos\left(\frac{n_y \pi y}{L_y}\right)$  or  $\cos\left(\frac{n_z \pi z}{L_z}\right)$  equal zero the pressure will be zero. These collections of points of zero pressure form nodal planes. The nodal patterns will vary depending on the size, shape and damping on the walls of a room. This means that certain speaker positions and certain listening positions will determine the way a source is perceived at a given point.

To avoid notational confusion, we will henceforth refer to these eigenfunctions by using  $\psi_N$ , with the subscript  $N$  representing  $n_x n_y n_z$ .

We have previously stated in section 2 that  $kc = 2\pi f$ . This implies that the eigenfrequencies or modal frequencies are:

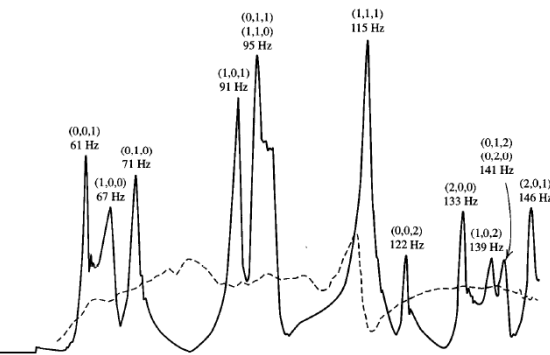
$$f_N = \frac{c}{2\pi} k_N . \quad (44)$$

## 5.2. Effect of the room modes

The effect of the room modes on the sound measured at a given point can be seen by comparing a sound source in a room where the walls are very heavily damped so that very little of the wave is reflected (an anechoic chamber) and a room with reflective walls (see figure 7). The peaks in the graph relating to the room with reflective walls represents the modal frequencies.

Only if a speaker is placed at an antinode, can the normal mode be fully excited (Kinsler, 2000, p. 353). This is exactly equivalent to the tuning fork example given above in section 2. If the speaker is located at a node, then the mode will excite the normal mode very little. Similarly, if listener is located at a node, the sound pressure will change very little, but if they are at an anti-node the pressure change will be at its maximum.

Figure 7  
Image: (Kinsler, 2000, p. 354)



A graph which shows amplitude against frequency for an anechoic chamber (dotted line) and a room with reflective walls (solid line). The sharp peaks represent the resonant frequencies.

### 5.3. Modal density

It can be seen from the graph in figure 7 that amplitude spikes caused by modal frequencies have a certain bandwidth. This is because frequencies within a certain finite range of the modal frequency will have the effect of significantly increasing the pressure difference. Clearly, if there were a sufficient number of these in a given bandwidth they would begin to overlap. When this happens, the effect of the room modes becomes less noticeable. This ‘flat response’ is what is considered desirable in a good listening room. However, if the modal frequencies are many Hertz apart, there is unlikely to be any overlap and certain frequencies will resonate more strongly than others. This is what designers of good listening rooms seek to avoid.

To estimate the likelihood of the modal frequencies overlapping, modal density is calculated. Modal density is defined as the number of modal frequencies per Hz.

It can be shown that the number of eigenfrequencies up to a frequency  $f$  is equal to:

$$N_f = \frac{4\pi}{3}V\left(\frac{f}{c}\right)^3 + \frac{\pi}{4}S\left(\frac{f}{c}\right)^2 + \frac{L}{8c}f, \quad (45)$$

where,  $V$  is the volume of the room,  $S$  is the total surface area of the walls and  $L$  is equal to the sum of the lengths of the edges of the room (Kuttruff, 2009, p.78).

For a small rectangular room with dimensions 6m x 3m x 2m and a maximum frequency of 100 Hz, we find there are less than 15 eigenfrequencies. This equates to an average modal density of one eigenfrequency for 6.69 Hz. It is clear from the formula for the number of frequencies up to a given frequency (45) that modal density will increase rapidly as  $f$  increases. Schroeder (1962, p. 1820) has derived a formula for calculating the limit of the frequencies for which the average spacing of normal modes is smaller than one third of their bandwidth:

$$f_s \geq 2000 \left(\frac{RT_{60}}{V}\right)^{\frac{1}{2}}, \quad (46)$$

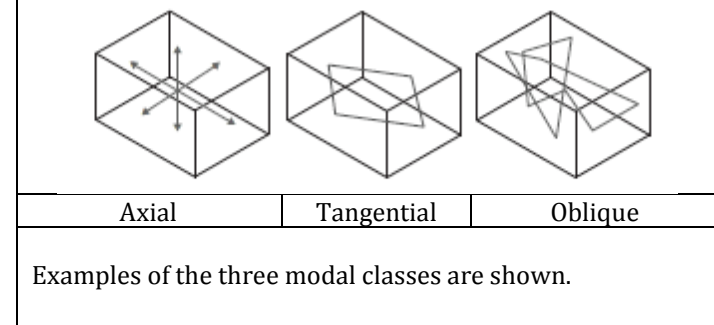
where  $RT_{60}$  is the reverberation time at a given frequency and is defined as the time taken for sound to decay by 60 dB.

In this project, the term “small rooms” has been used to describe the space we are interested in studying. We now have a way of identifying how “small” the room is. A small room is one where the modal density of the range of bass notes audible by humans falls below Schroeder’s limit.

## 5.4. Classes of room mode

When looking at the resonant frequencies of a tuning fork at the entrance of a pipe we effectively treated the situation as a one dimensional problem. The wave merely bounced off one wall and returned. In three dimensions the modes are more complicated. There are three types of mode; axial, tangential and oblique (Morse, 1948, p. 392). Examples of these can be seen in figure 8 and are described below:

Figure 8  
Image: (Laukkanen, 2014, p. 8)



Axial waves (Involve two parallel walls):

x-axial wave, parallel to the x-axis ( $n_y, n_z = 0$ )

y-axial wave, parallel to the x-axis ( $n_x, n_z = 0$ )

z-axial wave, parallel to the x-axis ( $n_x, n_y = 0$ )

Tangential waves (Involve 4 walls):

y,z-tangential waves, parallel to the y,z-plane ( $n_x = 0$ )

x,z-tangential waves, parallel to the x,z-plane ( $n_y = 0$ )

x,y-tangential waves, parallel to the x,y-plane ( $n_z = 0$ )

Oblique waves (involve all walls):

$n_x \neq 0, n_y \neq 0, n_z \neq 0$

In physical terms, the type of mode is very important. Each different type of mode has a different amount of energy. To explain this we first have to understand the principles of orthogonality.

## 5.5. Orthogonality and completeness of eigenfunctions

A useful feature of the eigenfunctions is that they form a complete and mutually orthogonal set.

The fact they are complete means we can express any sound pressure field in a given room as a linear combination of these eigenfunctions. For example, a source function  $q(x, y, z)$  can be expressed as:

$$q(x, y, z) = \sum_N A_N \psi_N(x, y, z) , \quad (47)$$

with suitably chosen coefficients  $A_N$ . To simplify notation, we again use the subscript  $N$  to represent  $n_x n_y n_z$ .

To understand the nature of orthogonality, we first consider the following identity:

$$\int_0^{L_x} \cos\left(\frac{n_x \pi}{L_x}\right) \cos\left(\frac{m_x \pi}{L_x}\right) dx = \begin{cases} L_x & \text{if } n_x = m_x = 0 \\ \frac{L_x}{2} & \text{if } n_x = m_x \neq 0 \\ 0 & \text{if } n_x \neq m_x \end{cases} \quad (48)$$

The proof of this is a straightforward matter of integration by parts. If the eigenfunctions are

$$\psi_N(x, y, z) = G_N \cos\left(\frac{n_x \pi x}{L_x}\right) \cos\left(\frac{n_y \pi y}{L_y}\right) \cos\left(\frac{n_z \pi z}{L_z}\right) \quad (49)$$

and

$$\psi_M(x, y, z) = H_M \cos\left(\frac{m_x \pi x}{L_x}\right) \cos\left(\frac{m_y \pi y}{L_y}\right) \cos\left(\frac{m_z \pi z}{L_z}\right), \quad (50)$$

where  $G_N$  and  $H_M$  are arbitrary coefficients then the volume integral of their product is

$$\iiint_V \psi_N(x, y, z) \psi_M(x, y, z) dV = \begin{cases} 0 & \text{for } N \neq M \\ G_N H_M L_x L_y L_z \epsilon_{n_x} \epsilon_{n_y} \epsilon_{n_z} & \text{otherwise} \end{cases} \quad (51)$$

where  $\epsilon_{n_x} = \begin{cases} 1 & \text{if } n_x = 0 \\ 2 & \text{if } n_x \neq 0 \end{cases}$  and  $\epsilon_{n_y}$  and  $\epsilon_{n_z}$  are similarly defined.

## 5.6. Energy of modes

The energy of a standing wave can be written as follows (Morse, 1948, p.402):

$$W_N = \frac{1}{2} \iiint_V \left( \rho v^2 + \frac{1}{\rho c^2} p^2 \right) dV \quad (52)$$

Replacing  $p$  with the eigenfunction  $\psi_N$  and relying on the orthogonality of the eigenfunctions tells us that:

$$W_N = \frac{V}{2 \epsilon_{n_x} \epsilon_{n_y} \epsilon_{n_z} \rho c^2}. \quad (53)$$

It can therefore be seen that axial waves have the most energy:  $\frac{V}{4\rho c^2} p^2$ , whilst oblique have the least:  $\frac{V}{16\rho c^2} p^2$ . This will automatically be taken into account in the mode summation method explored below.

## 6. Mode summation method

We have derived a formula to find the room modes. However, we want to find an equation that will approximate the sound pressure field at all points in the room when a source is used. To do this we need to solve the inhomogeneous Helmholtz equation:

$$\nabla^2 p(\mathbf{r}) + k^2 p(\mathbf{r}) = -i\omega q(\mathbf{r}), \quad (54)$$

where  $k = \frac{\omega}{c}$  and  $\mathbf{r}(x, y, z)$  is a position vector.

As explained above in section 5.5, eigenfunctions form a complete set of mutually orthogonal functions. This enables us to represent  $q(\mathbf{r})$  as a sum of eigenfunctions:

$$q(\mathbf{r}) = \sum_n A_N \psi_N(\mathbf{r}), \quad (55)$$

where

$$A_N = \frac{\epsilon_{n_x} \epsilon_{n_y} \epsilon_{n_z}}{V} \iiint_V \psi_N(\mathbf{r}) q(\mathbf{r}) dV. \quad (56)$$

We can also write the frequency dependent solution we seek,  $p(\mathbf{r})$ , in terms of a sum of eigenfunctions:

$$p(\mathbf{r}) = \sum_N B_N \psi_N(\mathbf{r}). \quad (57)$$

We substitute these equations in to the Helmholtz equation (54) which implies that

$$\sum_N A_N \left( \frac{\partial^2 \psi_N}{\partial x^2} + \frac{\partial^2 \psi_N}{\partial y^2} + \frac{\partial^2 \psi_N}{\partial z^2} + k^2 \psi_N \right) = -i\omega \rho_0 \sum_N B_N \psi_N(\mathbf{r}). \quad (58)$$

From the separated form of the inhomogeneous wave equation (37) and its relation to wave number  $k$  (38), we know that for eigenfunctions,  $\nabla^2 \psi_N = -k_N^2 \psi_N$ . We can relate therefore  $A_n$  and  $B_n$  as follows:

$$A_N = i\omega \rho_0 \frac{B_N}{k_N^2 - k^2}. \quad (59)$$

A point source located at  $\mathbf{r}_0$  can be represented simply by use of the delta function:

$$q(\mathbf{r}) = Q \delta(\mathbf{r} - \mathbf{r}_0), \quad (60)$$

where  $Q$  is the volume velocity of a sinusoidal source. The volume velocity measures the volume of airflow per unit time with units of  $m^3/s$ .

A property of the delta function is that

$$\int_{-\infty}^{+\infty} f(x) \delta\{dx\} = f(0). \quad (61)$$

Therefore substituting the equation for the point source (60) into that for  $A_N$  (56) gives us

$$A_N = \frac{\epsilon_{n_x} \epsilon_{n_y} \epsilon_{n_z}}{V} Q \psi_N(\mathbf{r}_0) \quad (62)$$

This implies that

$$p(\mathbf{r}) = i\omega Q \rho_0 \sum_N \frac{\epsilon_{n_x} \epsilon_{n_y} \epsilon_{n_z} \psi_N(\mathbf{r}) \psi_N(\mathbf{r}_0)}{V(k_N^2 - k^2)}, \quad (63)$$

Which is known as the Green's function of the room.

Earlier we showed that the eigenvalues and eigenfunctions for a room with rigid walls were

$$k_N = \left[ \left( \frac{n_x \pi}{L_x} \right)^2 + \left( \frac{n_y \pi}{L_y} \right)^2 + \left( \frac{n_z \pi}{L_z} \right)^2 \right]^{\frac{1}{2}} \text{ and } \psi_N = C \cos\left(\frac{n_x \pi x}{L_x}\right) \cos\left(\frac{n_y \pi y}{L_y}\right) \cos\left(\frac{n_z \pi z}{L_z}\right), \text{ respectively.}$$

If these values are used this equation approximates the pressure at all points in a room with rigid walls.

In the case of the room with rigid walls, the eigenvalues are real due to the relevant boundary conditions given at (39). By the definition of angular frequency (1) we can therefore write

$k_N = \frac{\omega_N}{c}$ , where  $\omega_N$  is the resonant angular frequency and  $c$  is the speed of light. The walls in a real room will be absorbent and will therefore have different boundary conditions. The eigenvalues of a room with absorbent walls are generally complex, we can therefore write  $k_N$  as:

$$k_N = \frac{\omega_N}{c} + i \frac{\delta_N}{c}, \quad (64)$$

where  $\omega_N$  is the real part of the resonant angular frequencies and  $\delta_N$  is the complex part.  $\delta_N$  relates to the absorbency of the walls and can be thought of as damping constants. If the walls are only lightly damped, then we expect  $\delta_n$  to be much smaller than  $\omega_n$ .

Making the assumption that  $\delta_n \ll \omega_n$  means that we can neglect  $\delta_n^2$  compared with  $\omega_n^2$  implying that

$$p(\mathbf{r}) = \frac{\omega c^2 Q \rho_0}{V} \sum_N \frac{\epsilon_{n_x} \epsilon_{n_y} \epsilon_{n_z} \psi_N(\mathbf{r}) \psi_N(\mathbf{r}_0)}{(\omega^2 - \omega_N^2 - 2i\delta_N\omega_N)}. \quad (65)$$

Clearly, when  $\omega$  approaches  $\omega_N$ , the denominator will become small causing  $p$  to rise significantly. These values of  $\omega_n$  correspond to the modal frequencies described above.

It can be shown that a first order approximation of the damping term  $\delta_n$  is given by (Morse, 1948, p. 405).

$$\delta_N = \frac{c}{8V} \left( \frac{1}{2} \epsilon_{n_x} \alpha_x + \frac{1}{2} \epsilon_{n_y} \alpha_y + \frac{1}{2} \epsilon_z \alpha_z \right) \quad (66)$$

where  $\alpha_x$  = average absorption coefficient of walls perpendicular to the  $x$  axis and  $\alpha_y$  and  $\alpha_z$  are similarly defined.

Assuming that the amount of damping is low, we can use the resonant angular frequencies  $\omega_N$  and eigenfunctions  $\psi_N$  calculated for the room assuming rigid wall to imply that

$$p(\mathbf{r}) = \frac{Q\omega c^2 \rho_0}{V} \sum_N \frac{\epsilon_{n_x} \epsilon_{n_y} \epsilon_{n_z} \psi_N(\mathbf{r}) \psi_N(\mathbf{r}_0)}{(\omega^2 - \omega_N^2 - 2i\delta_N \omega_N)}. \quad (67)$$

This equation approximates the steady state sound pressure field in a rectangular room with lightly damped walls.

## 6.1. MATLAB implementation of modal summation method

We have implemented the above modal sum method into MATLAB (Mathworks, 2015). The method is a straight forward one to code and is incredibly quick to run. In section 5.3 we showed that in a small room with low frequency sound waves, there will be relatively few room modes. This means that only a small number of calculations will have to be made to find all the relevant modes. Running the programme at 1 Hz intervals between 0 and 250 Hz for a given location in the room takes only a matter of seconds.

To make the output easier to analyse, a smoothing function has been applied. This averages the signal over  $1/n$  of an octave.  $1/12^{\text{th}}$  of an octave smoothing was found to be most appropriate in this case. A smoothing function code written by Christopher Hummerson (2016) was used to accomplish this.

The MATLAB code of the modal summation method implementation can be found online at <https://github.com/EvanTurnill/Acousticproject.git>.

## 7. Reflectance, absorption and impedance

In deriving the mode summation method, we assumed either that the boundaries were rigid or that any absorption of the walls was minimal. This will not always be realistic. The graph in figure 7 shows how significant the impact of highly damped walls can be. To provide a better approximation of the pressure field in the room we will therefore have to look more carefully at what happens at the boundaries of the room. This section follows Kutruff (2009, pp.36-43).

We will again treat the soundwave as a plane wave at the boundary. In fact, sources are more appropriately modelled as a point source producing spherical pressure waves. However, the interactions with an absorbent boundary would be very difficult to model. Further, so long as the source is a reasonable distance from the wall, the spherical wave will have expanded sufficiently to appear locally like a plane wave at the boundary. This is therefore a reasonable approximation.

To further simplify the problem, when calculating absorbency we will also assume the wall is infinite in length. Near the edges of the room, this will not be accurate, but it will be a reasonable assumption further from those points.

First, we define the absorption coefficient  $\alpha$  of the wall as the fraction of the incident energy lost during the reflection.  $\alpha$  takes a value of between zero and one. If  $\alpha$  equals one then all energy has been absorbed meaning there is no reflection. In this case, the boundary is so absorbent that the waves inside a room behave exactly as they would if there were no walls at all. If  $\alpha$  equals zero then no energy is lost. If the walls are rigid, this means there will be an in phase reflection. Between these values of  $\alpha$ , the reflected wave will change in both phase and amplitude. These changes can be represented by a complex reflection factor  $R = |R|e^{i\chi}$ . So for example, if an incident wave  $p_{in} = \hat{p}e^{i(\omega t+kx)}$  then the reflected wave would be described by  $p_r = R\hat{p}e^{i(\omega t+kx)}$  where  $\hat{p}$  is the maximum amplitude of the wave.

It can be shown that the intensity of a plane wave is proportional to the square of the pressure amplitude (Kuttruff, 2009, p.14) and therefore the intensity of the reflected wave will be  $|R|^2$  less than the intensity of the incoming wave. We can therefore write the absorbent coefficient as  $\alpha = 1 - |R|^2$ .

Another measure of the reflective characteristics of a wall is the wall impedance, which is defined as

$$Z = \left( \frac{p}{v_n} \right)_{surface}, \quad (68)$$

where  $v_n$  equals the velocity component normal to the boundary.  $Z$  is a complex value and will depend on the angle of incidence with the wall and the frequency of the wave. This can be related to both the reflection factor and to the absorption coefficient.

When deriving the wave equation, we showed that  $\rho_0 \frac{\partial v}{\partial t} + \nabla p = 0$  (26). If we again consider a plane wave moving in the  $x$  direction described by  $p_{in} = \hat{p}e^{i(\omega t+kx)}$ , then this implies that the particle velocity will be given by  $v_{in} = \frac{\hat{p}}{\rho_0 c} e^{i(\omega t+kx)}$ . The reflected wave will then be described by

$$p_r = R\hat{p}e^{i(\omega t+kx)} \text{ and } v_r = -R \frac{\hat{p}}{\rho_0 c} e^{i(\omega t+kx)}. \quad (69)$$

At  $x = 0$  these become

$$p_r = \hat{p}(1 + R)e^{i\omega t} \text{ and } v_r = \frac{\hat{p}}{\rho_0 c}(1 - R)e^{i\omega t}. \quad (70)$$

The impedance of the wall is given by dividing these two expressions, which implies that

$$Z = \rho_0 c \frac{1 + R}{1 - R} \Leftrightarrow R = \frac{Z - \rho_0 c}{Z + \rho_0 c}. \quad (71)$$

This can be related to the absorption coefficient by the fact that  $\alpha = 1 - |R|^2$ , which implies that

$$Z = \rho_0 c \frac{1 + \sqrt{1 - \alpha}}{1 - \sqrt{1 - \alpha}} \quad (72)$$

An alternate expression for the characteristics of a wall is known as the specific impedance which we will represent by  $\xi$  and which is defined as

$$\xi = \frac{Z}{\rho_0 C} \quad (73)$$

It can also be shown, using a similar method, that if the incident wave is at an oblique angle  $\theta$  to the wall (Kuttruff, 2009, p.43):

$$Z = \frac{\rho_0 c}{\cos \theta} \frac{1+R}{1-R} \Leftrightarrow R = \frac{Z \cos \theta - \rho_0 c}{Z \cos \theta + \rho_0 c}. \quad (74)$$

Having considered what happens at the boundary of a room with non-rigid walls, we can use this information to develop boundary conditions to use in an alternate model of the sound pressure field.

## 8. Finite difference time domain method (FDTD)

An alternate way of finding an approximation of the sound pressure field in a room with a source is to use finite difference equations.

We start with the time dependent scalar wave equation:

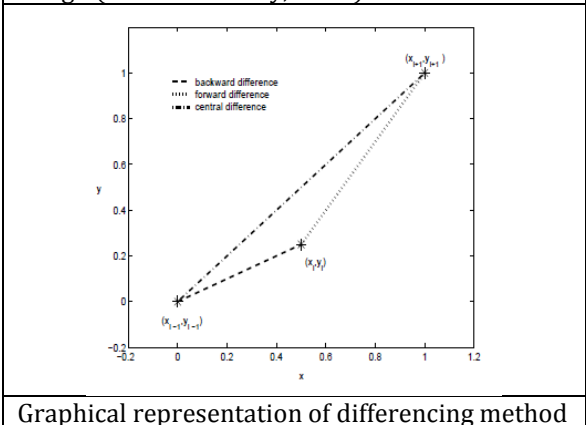
$$\frac{\partial^2 p}{\partial t^2} - c^2 \nabla^2 p = \frac{\partial q}{\partial t}. \quad (75)$$

To model this numerically requires the partial derivatives to be approximated. This can be done by the use of finite differences.

### 8.1. Finite differences

Finite difference methods approximate derivatives by using forward, backward or central differencing (Ohio University, 2015). We let  $y = f(x)$  and suppose that we know  $f$  at a finite set of points  $(x_1, y_1), (x_2, y_2), \dots, (x_n, y_n)$ . We also assume that the  $x$  coordinates are evenly spaced such that  $x_{i+1} - x_i = h$ . The most obvious way to approximate the derivative of  $f$  at  $x_0$  is to find the slope of the line which joins the point at  $x_0$  and those adjacent to it. This is known as forward or backward differencing. A visualisation of these methods can be seen at figure 9.

Figure 9  
Image:(Ohio University, 2015)



Graphical representation of differencing method

The forward differencing approximation of the derivative of  $f$  is

$$f'(x_i) = y'_i \approx \frac{y_{i+1} - y_i}{x_{i+1} - x_i} = \frac{y_{i+1} - y_i}{h}. \quad (76)$$

The backward differencing approximation of the derivative of  $f$  is

$$f'(x_i) = y'_i \approx \frac{y_i - y_{i-1}}{h}. \quad (77)$$

Central differencing is essentially the averaging of forward and backward differencing, which is given by

$$f'(x_i) = y'_i \approx \frac{y_{i+1} - y_{i-1}}{x_{i+1} - x_{i-1}} = \frac{y_{i+1} - y_{i-1}}{2h} \quad (78)$$

Taylor's theorem can be used to calculate the accuracy of these approximations. This states that

$$f(x_0 + h) = f(x_0) + hf'(x_0) + \frac{h^2}{2}f''(x_0) + O(h^3), \quad (79)$$

where  $O(h^3)$  indicates terms of the order  $h^3$ . Solving for  $f'(x)$  gives us that

$$f'(x_0) = \frac{f(x_0 + h) - f(x_0)}{h} + O(h) = \frac{y_{i+1} - y_i}{h} + O(h), \quad (80)$$

which is the forward difference equation plus terms of order  $h$ . This approximation is therefore first order accurate. We can again use Taylor's Theorem to show that backwards differencing is also first order accurate. By Taylor's theorem:

$$f(x_0 - h) = f(x_0) - hf'(x_0) + \frac{h^2}{2}f''(x_0) + O(h^3) \quad (81)$$

This can be rearranged to give:

$$f'(x_0) = \frac{f(x_0) - f(x_0 - h)}{h} + O(h) = \frac{y_i - y_{i-1}}{h} + O(h), \quad (82)$$

confirming that it is indeed first order.

Adding together the Taylor expansions of the forward (80) and backward differencing methods(82) and solving for  $f'(x_0)$  implies that

$$f'(x_0) = \frac{f(x_0 + h) - f(x_0 - h)}{2h} + O(h^2). \quad (83)$$

This shows that the central difference approximation is second order accurate. This is the differencing we will use to approximate the wave equation.

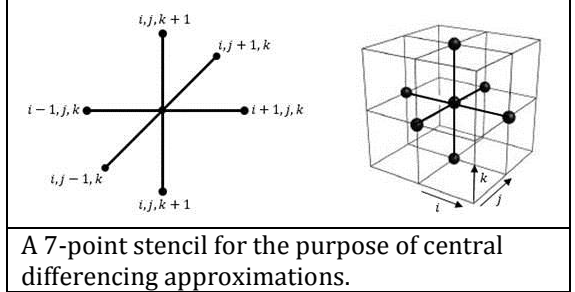
A second derivative can be derived by repeated central differencing, which implies that

$$\begin{aligned}
 f''(x_0) &\approx \frac{f'(x_0 + h) - f'(x_0 - h)}{2h} + O(h^2) \\
 &\approx \frac{(f(x_0 + 2h) - f(x_0)) - (f(x_0) - f(x_0 - 2h))}{h^2} + O(h^2). \\
 &= \frac{f(x_0 + 2h) + f(x_0 - 2h) - 2f(x_0)}{h^2} + O(h^2).
 \end{aligned} \tag{84}$$

## 8.2. Discretisation

In order to use the finite difference approximation, we need to create a mesh to represent points in the room. In this project we choose to have the grid points evenly spaced. For each time step, each node in the three dimensional spatial grid must be updated. Here we use a 7-point stencil as shown in figure 10. Central differencing is then used to average the value of the six neighbouring nodes.

Figure 10  
Image: (Darbyshire, 2015)



We define  $p_{i,j,k}^n$  as the update variable with  $n$  being the time index and  $i,j,k$  the indices for the spatial directions  $x, y, z$ . We define  $\delta T$  as the time step and  $\delta X$  as the spatial step. The wave equation can therefore be written (Kowalczyk and van Walstijn, 2008, p.892) as

$$\begin{aligned}
 &\frac{p_{i,j,k}^{n+1} - 2p_{i,j,k}^n + p_{i,j,k}^{n-1}}{(\delta T)^2} \\
 &= c^2 \left( \frac{p_{i+1,j,k}^n - 2p_{i,j,k}^n + p_{i-1,j,k}^n}{(\delta X)^2} + \frac{p_{i,j+1,k}^n - 2p_{i,j,k}^n + p_{i,j-1,k}^n}{(\delta X)^2} \right. \\
 &\quad \left. + \frac{p_{i,j,k+1}^n - 2p_{i,j,k}^n + p_{i,j,k-1}^n}{(\delta X)^2} \right). \tag{85}
 \end{aligned}$$

Rearranging to find the pressure at a given point at time  $n + 1$  gives:

$$p_{i,j,k}^{n+1} = \lambda^2 (p_{i+1,j,k}^n + p_{i,j-1,k}^n + p_{i,j+1,k}^n + p_{i,j-1,k}^n + p_{i,j,k+1}^n + p_{i,j,k-1}^n - 6p_{i,j,k}^n) + 2p_{i,j,k}^n - p_{i,j,k}^{n-1}, \tag{86}$$

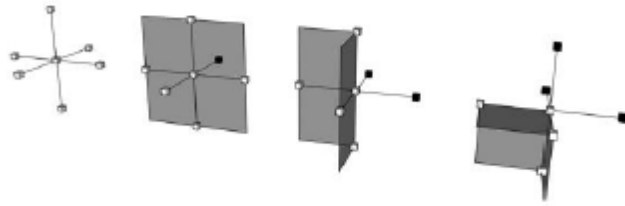
where  $= \frac{c \delta T}{\delta X}$ .  $\lambda$  is also known as the courant number. We choose  $\lambda = \sqrt{\frac{1}{3}}$  as it can be shown that this guarantees stability (Kowalczyk and van Walstijn, 2008, p.899). The sampling frequency of the system is  $f_s = \frac{1}{\delta T}$ , which means the model will approximate the pressure field  $\frac{1}{\delta T}$  times per second.

### 8.3. Boundary conditions

To find the specific solution to the wave equation we need to define initial boundary conditions.

At the boundary, the nodes do not have 6 adjacent nodes. Depending on whether a node is on a corner, an edge or a side, it will have one of the forms in figure 11. The nodes marked in black are known as ghost nodes. If we look at the central differencing method we have derived, we can see that when we try to update nodes on the boundary the algorithm will fail because these ghost nodes are undefined. We therefore need to define the ghost nodes by reference to an appropriate boundary condition so that the entire interior grid can be updated at every time step.

Figure 11:  
Image: (Haapaneimi, 2012, p.25)



A representation of the nodal connections of internal nodes, nodes on the side of the room, nodes on the edge of the room and nodes on the corner of the room. Each will be updated by use of 'ghost nodes' in the locations shown marked in black.

#### 8.3.1. Boundary points that are not on an edge or a corner

We will assume the boundary is locally reacting and is dependent only on location and frequency and not on the angle of incidence. We have previously shown at (26) that  $\rho_0 \frac{\partial v}{\partial t} + \nabla p = 0$ . Therefore, in the direction normal to the boundary

$$\rho_0 \frac{\partial v_n}{\partial t} + \frac{\partial p}{\partial n} = 0. \quad (87)$$

The definition of impedance (68) implies that at the boundary  $v_n = \frac{p}{Z}$ . Therefore

$$\frac{\rho_0}{Z} \frac{\partial p}{\partial t} + \frac{\partial p}{\partial n} = 0 \quad (88)$$

The definition of the specific wall impedance,  $\xi = \frac{Z}{\rho_0 c}$  (73) can be used to rewrite this as

$$\frac{\partial p}{\partial t} = -c\xi \frac{\partial p}{\partial n} \quad (89)$$

This is the appropriate boundary condition for the boundary nodes that are not corners or edges. For example, at the left and right boundaries in the  $x$  direction the boundary conditions are  $\frac{\partial p}{\partial t} = c\xi_{x_L} \frac{\partial p}{\partial x}$  and  $\frac{\partial p}{\partial t} = -c\xi_{x_R} \frac{\partial p}{\partial x}$  where  $\xi_{x_L}$  and  $\xi_{x_R}$  are the specific impedances of the relevant boundaries.

We can approximate the partial derivatives in the boundary condition with finite differences. Taking the right boundary in the  $x$  direction as an example:

$$\frac{p_{i,j,k}^{n+1} - p_{i,j,k}^{n-1}}{2\delta T} = -c\xi_{x_R} \frac{p_{i+1,j,k}^n - p_{i-1,j,k}^n}{2\delta X} \quad (90)$$

Solving for  $p_{i+1,j,k}^{n+1}$  gives:

$$p_{i+1,j,k}^n = p_{i-1,j,k}^n - \frac{\lambda}{\xi_{x_R}} (p_{i,j,k}^{n+1} - p_{i,j,k}^{n-1}) \quad (91)$$

This can then be substituted into the general update equation (86) to give the update equation for the right boundary as

$$\begin{aligned} p_{i,j,k}^{n+1} = & \lambda^2 \left( p_{i-1,j,k}^n - \frac{1}{\lambda \xi_{x_R}} (p_{i,j,k}^{n+1} - p_{i,j,k}^{n-1}) + p_{i,j-1,k}^n + p_{i,j+1,k}^n + p_{i,j-1,k}^n + p_{i,j,k+1}^n \right. \\ & \left. + p_{i,j,k-1}^n - 6p_{i,j,k}^n \right) + 2p_{i,j,k}^n - p_{i,j,k}^{n-1}, \end{aligned} \quad (92)$$

which can be rearranged to give that

$$\begin{aligned} p_{i,j,k}^{n+1} = & \frac{\lambda^2 (2p_{i-1,j,k}^n + p_{i,j+1,k}^n + p_{i,j-1,k}^n + p_{i,j,k+1}^n + p_{i,j,k-1}^n - 6p_{i,j,k}^n) + 2p_{i,j,k}^n + (\frac{1}{\lambda \xi_{x_R}} - 1)p_{i,j,k}^{n-1}}{\frac{1}{\lambda \xi_{x_R}} + 1}. \end{aligned} \quad (93)$$

### 8.3.2. Boundary points that are on an edge

These points will have to satisfy the wave equation and two boundary conditions. For example, the upper x-y edge will have to satisfy  $\frac{\partial p}{\partial t} = -c\xi_{x_R} \frac{\partial p}{\partial x}$  and  $\frac{\partial p}{\partial t} = -c\xi_{y_R} \frac{\partial p}{\partial y}$ . We therefore use the finite difference approximation of these boundary conditions to calculate the relevant ghost points. We then substitute this into the general update equation (86) to find the expression

$$\begin{aligned} p_{i,j,k}^{n+1} = & \frac{\lambda^2 (2p_{i-1,j,k}^n + 2p_{i,j-1,k}^n + p_{i,j,k+1}^n + p_{i,j,k-1}^n - 6p_{i,j,k}^n) + 2p_{i,j,k}^n + (\frac{\lambda}{\xi_{x_R}} + \frac{\lambda}{\xi_{y_R}} - 1)p_{i,j,k}^{n-1}}{\frac{\lambda}{\xi_{x_R}} + \frac{\lambda}{\xi_{y_R}} + 1}. \end{aligned} \quad (94)$$

### 8.3.3. Boundary points on a corner

The boundary points on the corner have to satisfy three boundary conditions. For example, the outermost corner must satisfy  $\frac{\partial p}{\partial t} = -c\xi_{x_R} \frac{\partial p}{\partial x}$ ,  $\frac{\partial p}{\partial t} = -c\xi_{x_R} \frac{\partial p}{\partial y}$  and  $\frac{\partial p}{\partial t} = -c\xi_{x_R} \frac{\partial p}{\partial z}$ . By the same method as used for the other types of boundary point, this gives

$$p_{i,j,k}^{n+1} = \frac{\lambda^2(2p_{i-1,j,k}^n + 2p_{i,j-1,k}^n + 2p_{i,j,k-1}^n - 6p_{i,j,k}^n) + 2p_{i,j,k}^n + (\frac{\lambda}{\xi_{x_R}} + \frac{\lambda}{\xi_{y_R}} + \frac{\lambda}{\xi_{z_R}} - 1)p_{i,j,k}^{n-1}}{\frac{\lambda}{\xi_{x_R}} + \frac{\lambda}{\xi_{y_R}} + \frac{\lambda}{\xi_{z_R}} + 1}. \quad (95)$$

## 8.4. Conversion to frequency domain

The above finite difference method gives an approximation of the pressure field for each time step. However, we want to analyse the sound pressure in the frequency domain. To obtain the steady state approximation we can use the discrete fourier transformation (“DFT”). The DFT converts a sequence of equally spaced samples into a finite combination of sine waves ordered by their frequencies (Discrete Fourier Transform, 2016). This can be implemented in MATLAB using the fast fourier transform algorithm (“FFT”). The inbuilt FFT function ‘fft’ has been used to carry out this process in my implementation (Mathworks, 1994).

## 8.5. MATLAB implementation of FDTD method

The code to implement the FDTD is somewhat more complicated than the modal summation method. It is also significantly slower. With a 5 second total time period and a sample rate of 2000 Hz the calculation of the sound field in the small room we are interested in requires approximately 12 minutes. One reason for this is that it needs to calculate the pressure at every node at every time step. One benefit of this is that after running the code, the pressure at every node, i.e. every position in the room, is obtained. However, assuming you only wish to measure the pressure field at a small number of positions, the modal summation method is much faster taking less than a minute to calculate the pressure at 18 combinations of speaker and microphone location.

As in the summation method, a 1/12<sup>th</sup> of an octave smoothing function was applied to make the output easier to analyse.

The MATLAB code of this implementation can be found at:

<https://github.com/EvanTurnill/Acousticproject.git>.

## 9. Actual measurement

### 9.1. The room

In order to evaluate the methods above, measurements have been taken of a real room. The room had the following measurements: Lx=2.950 m; Ly=6.105 m and Lz=2.260 m.

Unfortunately, the only room we had access to measure was not perfectly rectangular. There was a supporting beam measuring 0.2 m by 0.2 m located on the ceiling 1 m from the wall closest to the speaker. There was also a fireplace surround that protruded from the wall with dimensions of 0.2 m by 1 m by 1 m located 3.05 m from the wall nearest the speakers. The room also contained some furniture which it was not possible to remove. This included a small sofa of dimensions 2 m by 1m by 0.8 m which we placed against the furthest wall from the speaker and a chest of drawers of dimensions 1.5 m by 0.9 m by 0.6 m which was placed just under where the speaker were positioned. See figures 12,13 and 14 below for the layout of the room.

All of these features will have an impact on the measurements taken, particular at the higher frequencies which will be more prone to scattering upon contact with them.

### 9.2. The measurement method

A computer programme was used to play a ‘sweep’ of frequencies between 1 and 2000 Hz through the speaker in the room. The computer also measured the sound pressure in the room through an attached microphone. The programme then applied a fast Fourier transformation to obtain a graph of pressure against frequency. This is then smoothed in 12<sup>th</sup> octave intervals. The computer programme also calculated the reverberation time (RT60). The computer programme used was ARTA (Mateljan, 2015).The microphone used was an Earthworks M30.

### 9.3. The speaker and microphone positions

The speaker was placed at the following positions (all in metres):

Table 1			
	$x$	$y$	$z$
Speaker position 1	0.70	0.45	1.33
Speaker position 2	1.73	0.45	1.33
Speaker position 3	1.20	1.30	1.03
Speaker positions in the room under test.			

The microphone was placed at the following positions (all in metres):

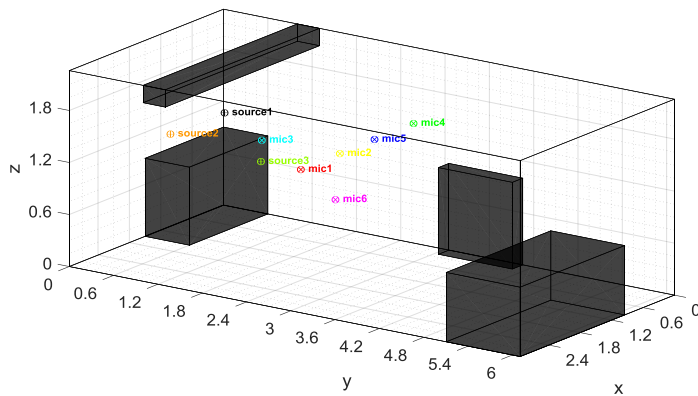
Table 2

	<i>x</i>	<i>y</i>	<i>z</i>
Microphone position 1	1.475	2.030	1.130
Microphone position 2	0.725	2.030	1.130
Microphone position 3	2.225	2.030	1.650
Microphone position 4	0.725	3.030	1.650
Microphone position 5	1.475	3.030	1.650
Microphone position 6	2.225	3.030	1.130

Microphone positions in the room under test.

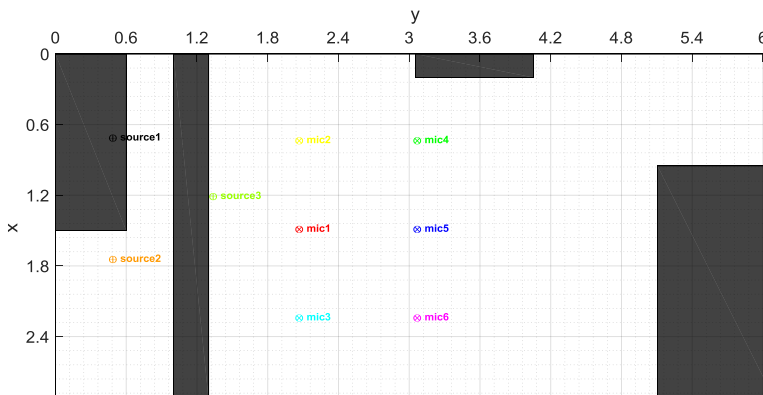
Each combination of these positions was tested, amounting to 18 measurements in total.

Figure 12



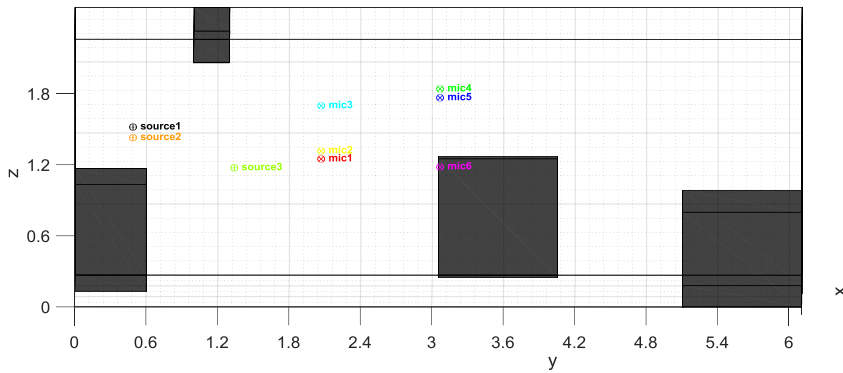
A 3-D representation of the room being measured including microphone and speaker positions.

Figure 13



A bird's eye view of the room being measured including microphone and speaker positions.

Figure 14:



A side-on view of the room being measured including microphone and speaker positions. The viewing position is slightly angled to enable the microphones and speakers that are at the same height to become visible.

#### 9.4. Calculation of absorption coefficients of the walls for use in implementations

If a listening room is being designed, calculations can be made of the likely absorption coefficients for each frequency range by reference to tables of absorption for commonly used material such as brick or plasterboard (Sengpie, 2014a).

If the room is already in existence, the reverberation time (RT60) time can be used to calculate the average absorption of the walls in the room. The RT60 rate is related to the absorption coefficient by an equation discovered by Wallace Sabin (Sengpie, 2014b).

$$RT60 = \frac{kV}{A} = 0.161 \frac{kV}{A} \quad (96)$$

where  $k = \frac{24 \ln 10}{c} = 0.161$ ,  $V$  is the room volume ( $m^3$ ),  $A = \alpha S$  is the average absorption of the room in *Sabins*,  $\alpha$  = absorption coefficient,  $S$  = absorbing surface area in  $m^2$  and  $c$  = speed of sound which is assumed to be  $343 m/s$ .

Using the calculated RT60 times we can therefore calculate the average absorption coefficient.

For this project, the RT60 was measured at 31.5Hz, 63Hz, 125Hz and 250Hz and the results were used to calculate the average absorption coefficient of the room at those frequencies. By way of linear interpolation, the absorption coefficients at all frequencies from 1 to 250Hz were then calculated to be used in the two implementations described above.

## 10. Results

### 10.1. Comparison of the models with actual measurements

When comparing the actual measurements taken to those calculated by the modal summation method, there is a strong visual similarity in most of the 18 combinations of speaker and microphone positions. Figure 15 shows an example where the pattern of peaks are closely related. However, as figure 16 demonstrates, the model provided a far less accurate approximation for some of the actual measurements taken.

The situation is similar with the FDTD results. Most of the 18 points of measurement show a reasonable correlation (see for example figure 17), particular up to about 120 Hz. However, some are very poor approximations. See for example figure 18.

We have made a number of assumptions in this case which could explain the difference between the actual and modelled results. Perhaps the most obvious of these is the fact we assumed the room was rectangular. In fact, as discussed above, the room had a beam, sofa, fireplace and chest of drawers (see figures 12-14) meaning the room was far from rectangular. It is difficult to be certain of the degree to which they would have affected the actual measurements taken. However, one thing we might expect to see if this was a factor is a closer correlation between the models and actual results where the microphone was placed as far from the irregular features in the room as possible. Microphones 5 and 6 are nearest the centre of the room. They are furthest away from the beam and a reasonable distance from the sofa. The measurements in these positions do provide the closest correlation of all the microphone positions (see figures 21-38 in the appendix for the amplitude frequency graphs for all positions). For comparison, microphone 3 is closest horizontally to the beam and is only 40cm below it. This appears to be the least well modelled position of microphone. We also note that speaker position 3 appears to be the least well modelled of the speaker positions. This is the lowest of the three positions and it may be most affected by the chest of drawers and sofa which are closest in height to this position.

We also made certain approximations regarding the acoustic properties of the boundaries which may explain the inaccuracy of the models. In the implementation of this project an average absorption coefficient was created by measuring the response time of the room. This is unrealistic as we would expect the carpeted floor and plasterboard/wood ceiling to be more absorbent than the plasterboard/brick walls. If the absorption coefficient is different on every wall, this will impact the results. This may also explain why the microphones furthest from the boundaries provide measurements closer to that predicted by the models.

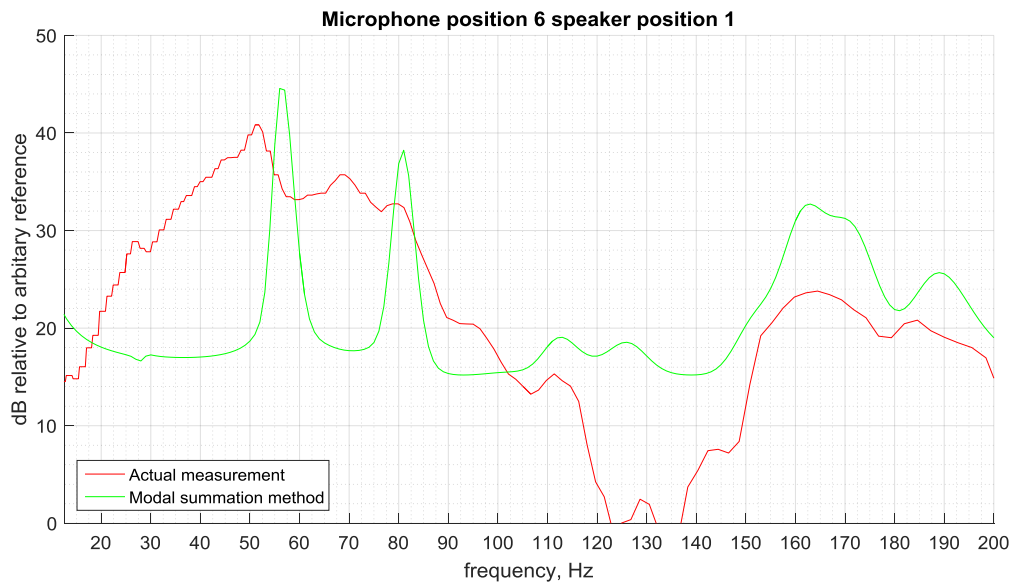
Further testing in a perfectly rectangular room would hopefully narrow down the reasons for differences between the models and actual measurements taken.

### 10.2. Differences between the two models

Something which is more difficult to explain is the differences between the two models. Both assume that the room is perfectly rectangular and that the absorbency of the walls is the same. We would therefore hope for a fairly good correlation between the two models. However, whilst

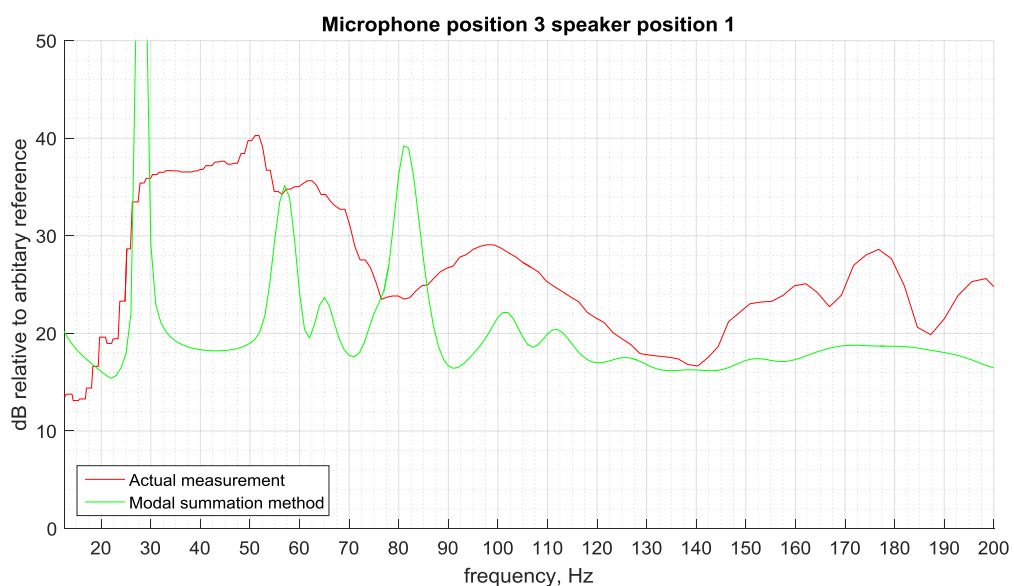
they are similar in terms of patterns of peaks, they are far from identical (see figures 19 and 20 below). This discrepancy may be explained by the fact that the mode summation method relies on the assumption that the damping is minimal, whereas the FDTD model does not. In the room that was measured, the absorption coefficients were not negligible, particularly at the higher frequencies. This may, in part, explain why the two models differ.

Figure 15:



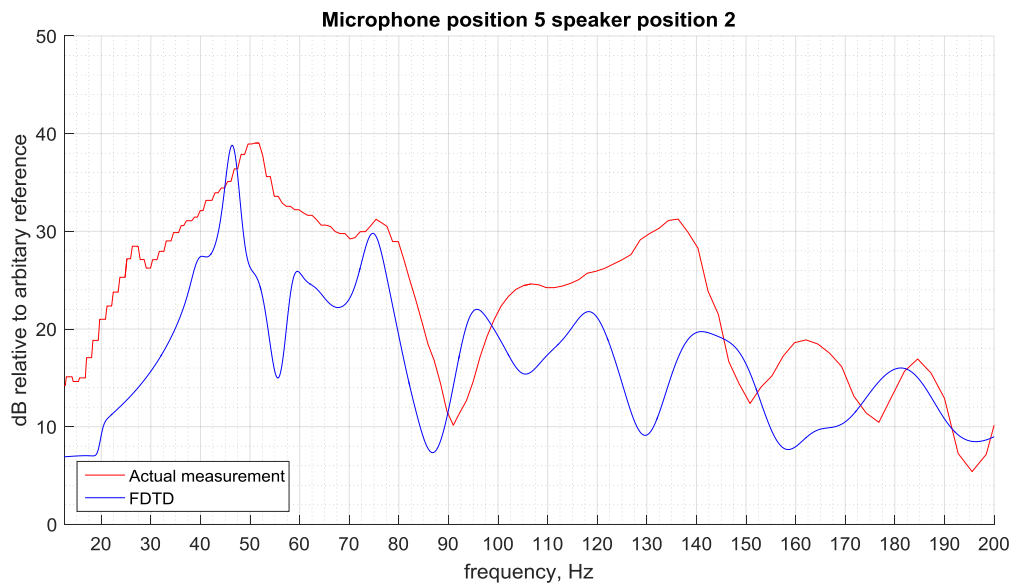
A plot of amplitude (dB) against frequency (Hz) for the actual measurements (red) and mode summation method (green) at microphone position 6 and speaker position 1. This is one of the positions that produced the closest correlation between the mode summation method and the actual results. Microphone 6 was the furthest from the boundaries and objects that may have distorted these results, such as the beam and furniture present in the room.

Figure 16:



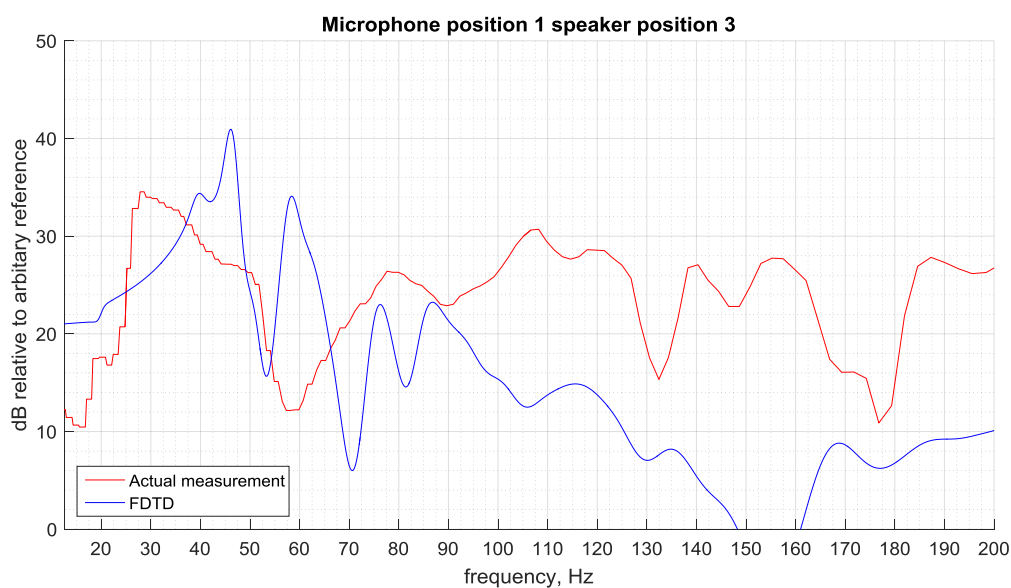
A plot of amplitude (dB) against frequency (Hz) for the actual measurements (red) and mode summation method (green) at microphone position 3 and speaker position 1. This is one of the positions where the correlation was far weaker. Microphone position 3 was closest to the beam in the room, which may have been part of the cause for the discrepancies.

Figure 17:



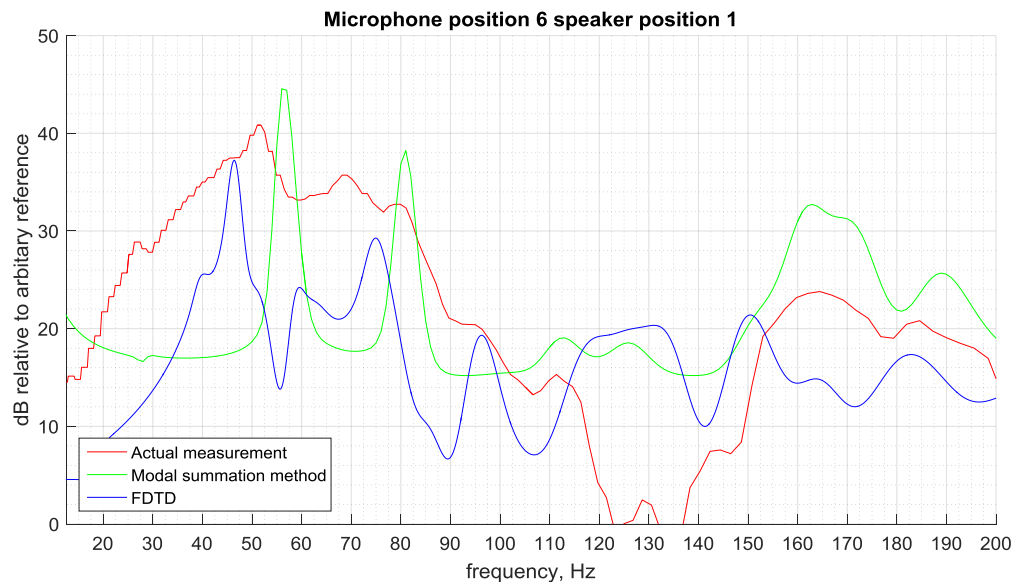
A plot of amplitude (dB) against frequency (Hz) for the actual measurements (red) and FDTD method (blue) at microphone position 5 and speaker position 2. This is one of the positions that produced the closest correlation between the FDTD and the actual results. Microphone 5 was one of those furthest from the boundaries and objects that may have distorted these results, such as the beam and furniture present in the room. This graph is representative of all those generated by the FDTD model, in that its accuracy seems to degenerate for frequencies over about 120Hz.

Figure 18:



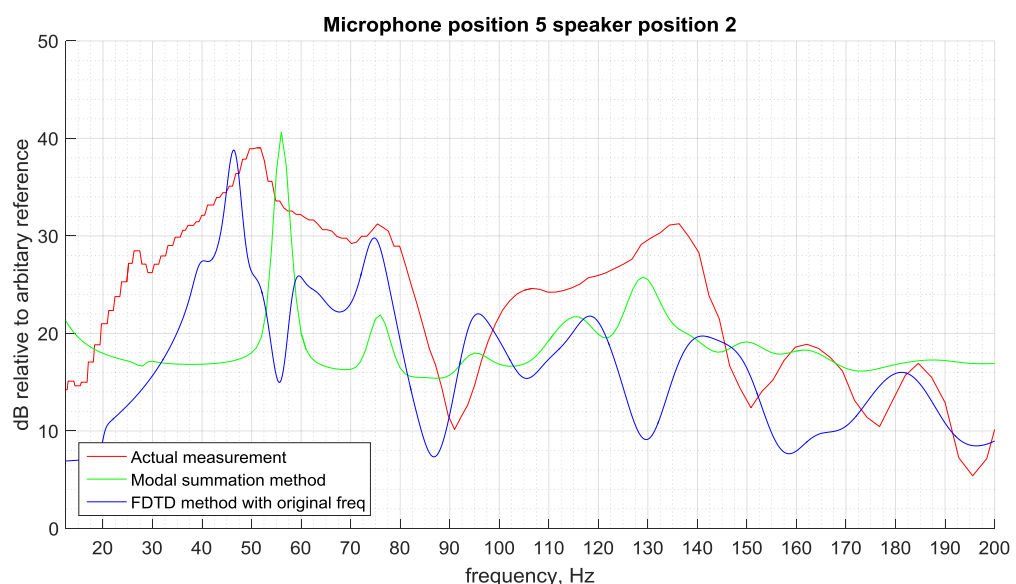
A plot of amplitude (dB) against frequency (Hz) for the actual measurements (red) and FDTD method (blue) at microphone position 3 and speaker position 1. This is one of the positions where the correlation was far weaker. Microphone position 3 was closest to the beam in the room, which may have been part of the cause for the discrepancies.

Figure 19:



A plot of amplitude (dB) against frequency (Hz) for the actual measurements (red) and mode summation method (green) and FDTD method (blue) at microphone position 6 and speaker position 1.

Figure 20:



A plot of amplitude (dB) against frequency (Hz) for the actual measurements (red), mode summation method (green) and FDTD method (blue) at microphone position 5 and speaker position 2.

## 11. Conclusion

In this project we have developed a detailed picture of what happens when a speaker is placed in an enclosed space. We derived the time-dependent wave equation and the time-independent Helmholtz equation and used them to explain the importance of modal frequencies to the experience of those listening to low frequency sound in small rooms. Finally, we have shown two ways of modelling a rectangular room and have implemented those models.

Both the mode summation and the FDTD models gave some indications of the difficulty of obtaining a flat bass response in small rooms and generated results that bore a reasonable correlation to the actual measurements. This was particularly the case at microphone and speaker positions that were furthest from the boundaries, where they were least likely to be affected by the furniture in the room, the support beam or by assumptions made regarding the boundary conditions themselves. Further testing in a truly rectangular room may provide further insight into the reasons for the causes of the shortcomings of these models.

Although both models can give a very rough indication of the resonant frequencies that are likely to cause problems in a listening room, they are not sufficiently accurate to determine with certainty the perfect listening position or speaker location. We would therefore wish to develop a more accurate model.

One way to try and improve the accuracy of the results is to impose more accurate boundary conditions. For example, a boundary condition can be derived that models the walls as a combination of a spring-like boundary and a mass like boundary (Kowalczyk, 2008, p.895).

We could also seek to improve the approximation of the absorption coefficient by taking into account the fact that the absorption will vary on each wall. This can be done by estimating the absorption coefficient for each wall based on the materials it is made of. However, this too is far from an exact science. Walker, (1992, p.8), points out that accurate data relating to the acoustic properties of materials is very difficult to find and that, at low frequencies, materials may well have impedances which change significantly over narrow frequency bands.

Even if these steps were taken, this would not address the fact that most listening rooms will not be exactly rectangular. Like the room measured in this project, most will have features such as beams or fireplaces and will need furniture of some type. The FDTD method could be varied to account for these features. This would involve creating a mesh that reflects the shape of the room and identifying the necessary ghost points to enable the mesh to be updated. The mesh would still have to be made up of rectangles, but with sufficient numbers of rectangles, angled surfaces could be approximated. Trevor Cox (2015) has produced an example of how such a code may be implemented is. This example is only really a visualisation of the pressure field, but it demonstrates how the code used in this project could be adapted.

However, to generate meshes in this way will be difficult, particularly with curved objects. A different method called the Finite Element Method ("FEM") is more able to deal with this problem. This method is essentially a generalisation of the finite difference method above. It allows for a mesh with non-rectangular elements, which means it can model more complicated shapes more accurately than the FDTD method. However, it still has the disadvantage that all nodes have to be updated. This means it has significant computing time, particularly at the

higher frequencies where more nodes are needed to ensure stability. For small rooms such as those considered in this project, this may be a satisfactory method.

Another method that could be investigated is the Boundary Element Method (“BEM”). This can be used to solve problems for which Green’s functions can be calculated. The method uses given boundary conditions to calculate the boundary values of the integral equation. The interior points can then be worked out by using the integral equation to calculate the solution at the point of interest inside the room. Only needing to calculate the points on the boundary of the domain of interest has the potential to make it far more efficient than the finite element methods (Boundary Element Method, 2016). For a detailed explanation of BEM see (Brebbia, Dominguez, 1994). A comparison of the FEM and BEM methods can be found at (Tang, Zhou and Hui, 2006).

Accurate modelling of the propagation of sound waves will help architects design every space, from small home studios to auditoria, in a way that optimises the experience of those listening to sound in them. The current models available, though far more complex than those used in this project, do not always provide as much detail as architects would like. A great deal more research and development is therefore required from the acousticians, engineers and mathematicians who work in this field.

## References

- Acoustic theory* (2015) in *Wikipedia*. Available at:  
[https://en.wikipedia.org/wiki/Acoustic\\_theory](https://en.wikipedia.org/wiki/Acoustic_theory) (Accessed: 8 May 2016).
- Avis, M.R. (2000) *The active control of low frequency room modes*. Available at:  
<http://usir.salford.ac.uk/14820/1/DX236804.pdf> (Accessed: 8 May 2016).
- Boundary element method* (2016) in *Wikipedia*. Available at:  
[https://en.wikipedia.org/wiki/Boundary\\_element\\_method](https://en.wikipedia.org/wiki/Boundary_element_method) (Accessed: 8 May 2016).
- Brebbia, C.A. (1994) *Boundary elements: An Introduction*. Edited by J Dominguez. 2nd edn. Boston: WIT Press Computational Mechanics.
- Cox, T. (2015) *Acoustic FDTD example*. Available at:  
<http://www.mathworks.com/matlabcentral/fileexchange/53070-acoustic-fdtd-example> (Accessed: 8 May 2016).
- Darbyshire, P.M. (2015) '3D Visualisation of Tumour-Induced Angiogenesis using the CUDA programming model and OpenGL Interoperability: Science publishing group', *Science Publishing Group*, 3(5), p. 53. doi: 10.11648/j.jctr.20150305.11.
- Discrete Fourier transform* (2016) in *Wikipedia*. Available at:  
[https://en.wikipedia.org/wiki/Discrete\\_Fourier\\_transform](https://en.wikipedia.org/wiki/Discrete_Fourier_transform) (Accessed: 8 May 2016).
- Haapaniemi, A. (2012) *Simulation of acoustic wall reflections using the finite-difference time-domain method school of electrical engineering A?* Available at:  
<http://lib.tkk.fi/Dipl/2012/urn100652.pdf> (Accessed: 8 May 2016).
- Harmonics in a violin tone* (no date) Available at: <http://www.ccp14.ac.uk/ccp/web-mirrors/isotropy/~stokes/vwave.jpg> (Accessed: 8 May 2016).
- Hummersone, C. (2016) *File exchange - MATLAB central*. Available at:  
[http://www.mathworks.com/matlabcentral/fileexchange/55161-1-n-octave-smoothing/content/smooth\\_spectrum.m](http://www.mathworks.com/matlabcentral/fileexchange/55161-1-n-octave-smoothing/content/smooth_spectrum.m) (Accessed: 8 May 2016).
- Indiana University (no date) *PURE TONES*. Available at:  
<http://www.indiana.edu/~p1013447/dictionary/tone.htm> (Accessed: 8 May 2016).
- Interference (wave propagation)* (2016) in *Wikipedia*. Available at:  
[https://en.wikipedia.org/wiki/Interference\\_\(wave\\_propagation\)](https://en.wikipedia.org/wiki/Interference_(wave_propagation)) (Accessed: 8 May 2016).
- Introduction to physical chemistry – lecture 5 supplement: Derivation of the speed of sound in air* (no date) Available at:  
[https://upload.wikimedia.org/wikipedia/commons/e/eb/Introduction\\_to\\_Physical\\_Chemistry\\_Lecture\\_5\\_Supplement.pdf](https://upload.wikimedia.org/wikipedia/commons/e/eb/Introduction_to_Physical_Chemistry_Lecture_5_Supplement.pdf) (Accessed: 8 May 2016).
- Kinsler, L.E., Frey, A.R. and Coppens, A.B. (2000) *Fundamentals of acoustics*. 4th edn. United States: John Wiley and Sons (WIE).

Kowalczyk, K. and van Walstijn, M. (2008) 'Formulation of locally reacting surfaces in FDTD/K-DWM Modelling of acoustic spaces', *Acta Acustica united with Acustica*, 94(6), pp. 891–906. doi: 10.3813/aaa.918107.

Kuttruff, H. and Heinri, K. (2009) *Room acoustics*. 4th edn. New York, NY: Taylor & Francis.

Laukkanen, P. (2014) *Evaluation of studio control room acoustics with spatial impulse responses and Auralization*. Available at:  
[https://mediatech.aalto.fi/~ktlokki/Publs/mst\\_laukkanen.pdf](https://mediatech.aalto.fi/~ktlokki/Publs/mst_laukkanen.pdf) (Accessed: 8 May 2016).

M. Derbyshire, P. (2015) '3D Visualisation of Tumour-Induced Angiogenesis using the CUDA programming model and OpenGL Interoperability', *Journal of Cancer Treatment and Research*, 3(5), pp. 53–65. doi: 10.11648/j.jctr.20150305.11.

MacArthur, B. (2015) 'MATH3072 Biological Fluid Dynamics Outline Lecture Notes', Southampton: University of Southampton. .

Mateljan, I. (2015) ARTA (version 1.8.5). Available at: <http://www.artalabs.hr/> (Accessed: 11 May 2016).

Mathworks. (1994) *Fast Fourier transform (FFT)*. Available at:  
<http://uk.mathworks.com/help/matlab/math/fast-fourier-transform-fft.html> (Accessed: 8 May 2016).

Mathworks. (2015) MATLAB (2015b). Available at:  
<http://uk.mathworks.com/products/matlab/> (Accessed: 11 May 2016).

Morse, P. (1948) *Vibration and Sound*. 2nd edn. New York: McGraw-Hill Book Company Inc.

Ockendon, H. and Ockendon, J.R. (1995) *Viscous flow*. Cambridge: Cambridge University Press.

Ohio University (2015) *Lecture 27 numerical differentiation Approximating derivatives from data*. Available at: <https://www.math.ohio.edu/courses/math3600/lecture27.pdf> (Accessed: 8 May 2016).

Riley, K.F., Hobson, M.P. and Bence, S.J. (2006) *Mathematical methods for physics and engineering: A comprehensive guide*. 3rd edn. United Kingdom: Cambridge University Press.

Runborg, O. (2012) *Helmholtz equation and high frequency approximations*. Available at:  
<http://www.csc.kth.se/utbildning/kth/kurser/DN2255/ndiff12/Lecture5.pdf> (Accessed: 8 May 2016).

Schroeder, M.R. (1962) 'Frequency-Correlation functions of frequency responses in rooms', *The Journal of the Acoustical Society of America*, 34(12), pp. 1819–1823. doi: 10.1121/1.1909136.

Sengpiel, E. (2014a) *Absorption coefficients building materials finishes RT60 alpha coefficient acoustic absorbing absorbtion floor seating wall ceiling miscellaneous materials - sengpielaudio Sengpiel Berlin*. Available at: <http://www.sengpielaudio.com/calculator-RT60Coeff.htm> (Accessed: 8 May 2016).

Sengpiel, E. (2014b) *RT60 calculator Wallace C. Sabine calculation reverberation time Sabin Sanine's formula online sound pressure sound level - sengpielaudio Sengpiel Berlin*. Available at: <http://www.sengpielaudio.com/calculator-RT60.htm> (Accessed: 8 May 2016).

Stein, E.M. and Shakarchi, R. (2003) *Fourier analysis: An introduction*. United States: Princeton University Press.

Tang, Y.M., Zhou, A.F. and Hui, K.C. (2006) 'Comparison of FEM and BEM for interactive object simulation', *Computer-Aided Design*, 38(8), pp. 874–886. doi: 10.1016/j.cad.2006.04.014.

Textbook Equity (2014) *College physics textbook equity edition volume 2 of 3: Chapters 13 - 24*. United Kingdom: Lulu.com.

University of Salford (no date) *Principles of Sound Synthesis*. Available at: [http://www.acoustics.salford.ac.uk/acoustics\\_info/sound\\_synthesis/](http://www.acoustics.salford.ac.uk/acoustics_info/sound_synthesis/) (Accessed: 8 May 2016).

Walker, R. (1992) 'Low-Frequency Room Responses Part 1', *BBC Research Department Report*, 1992/9.

## Appendix

Figure 21

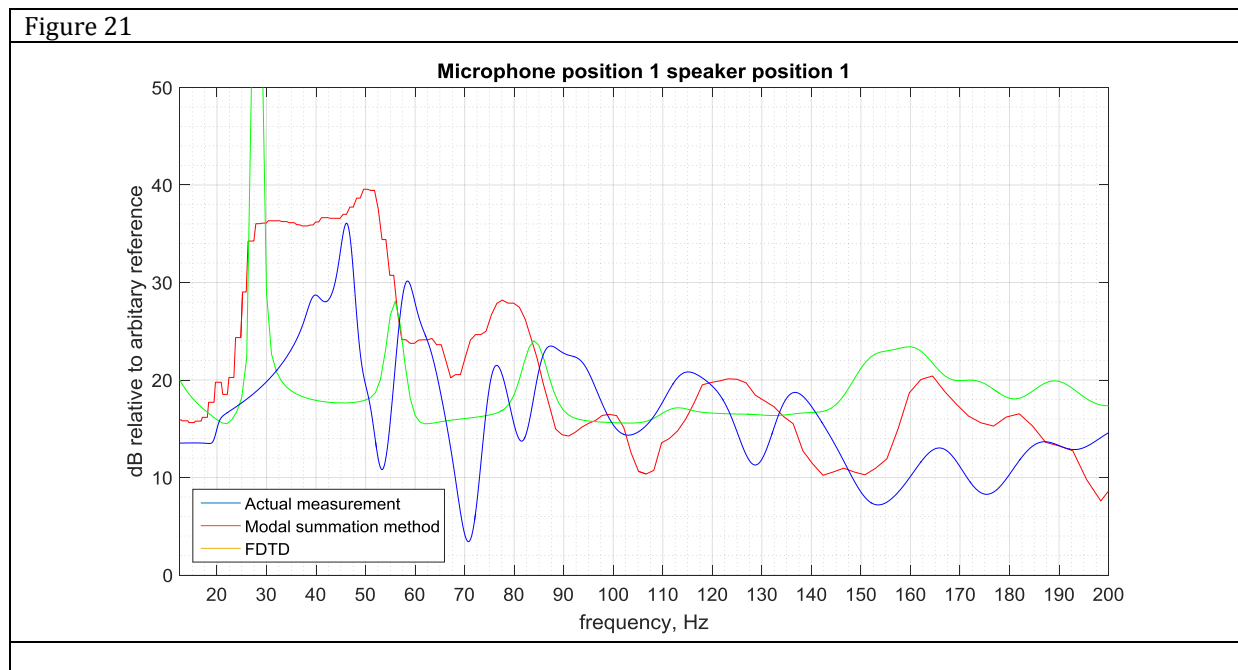


Figure 22

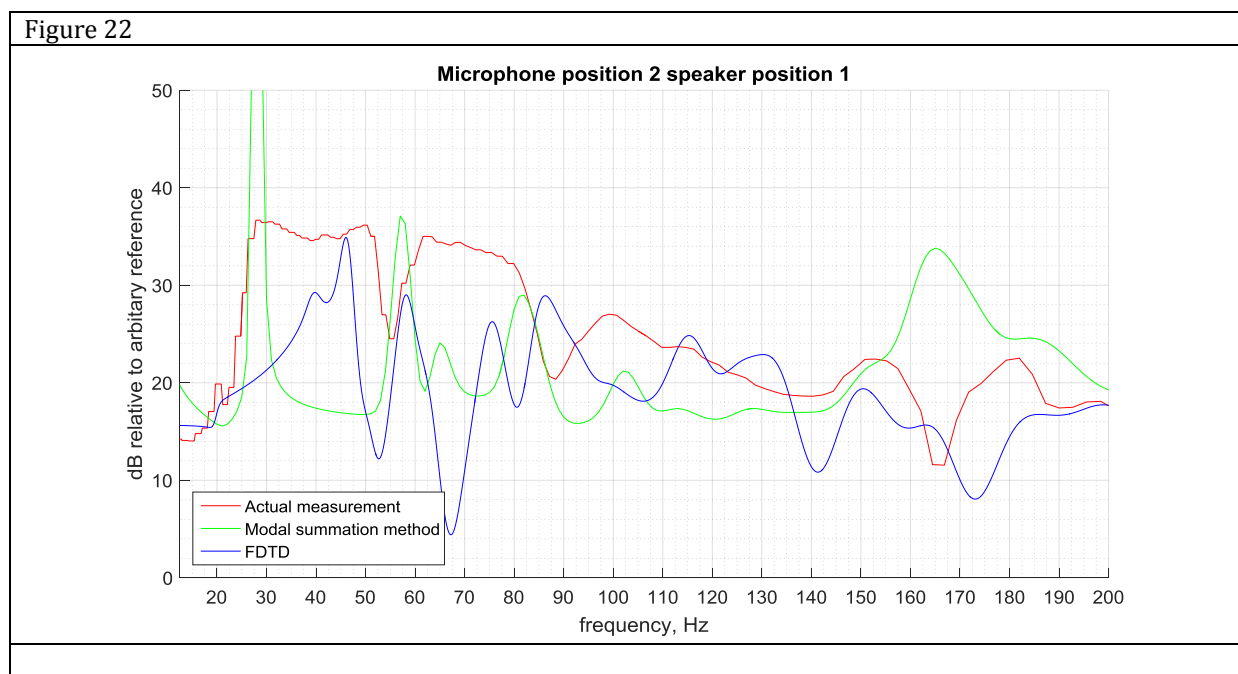


Figure 23

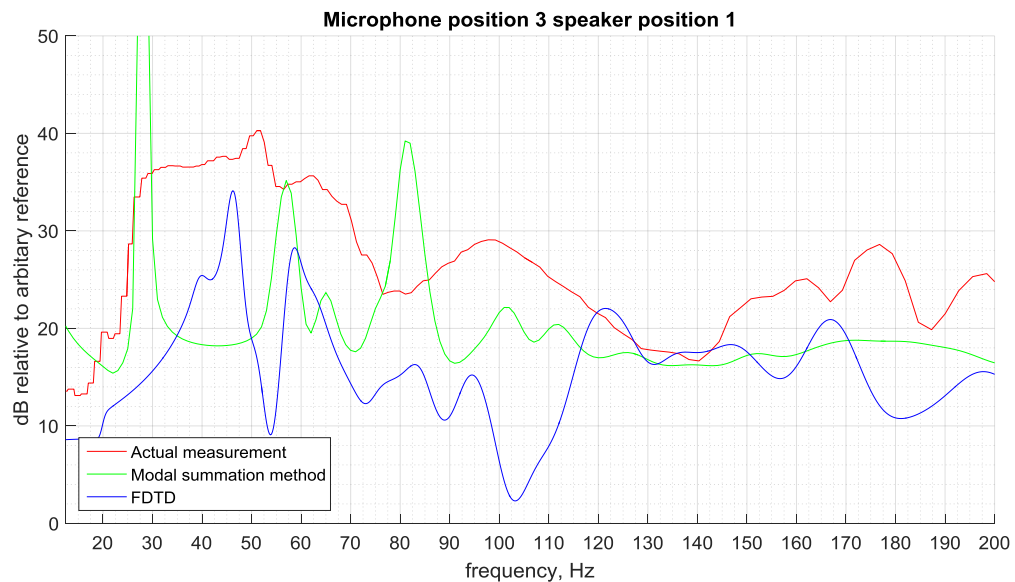


Figure 24

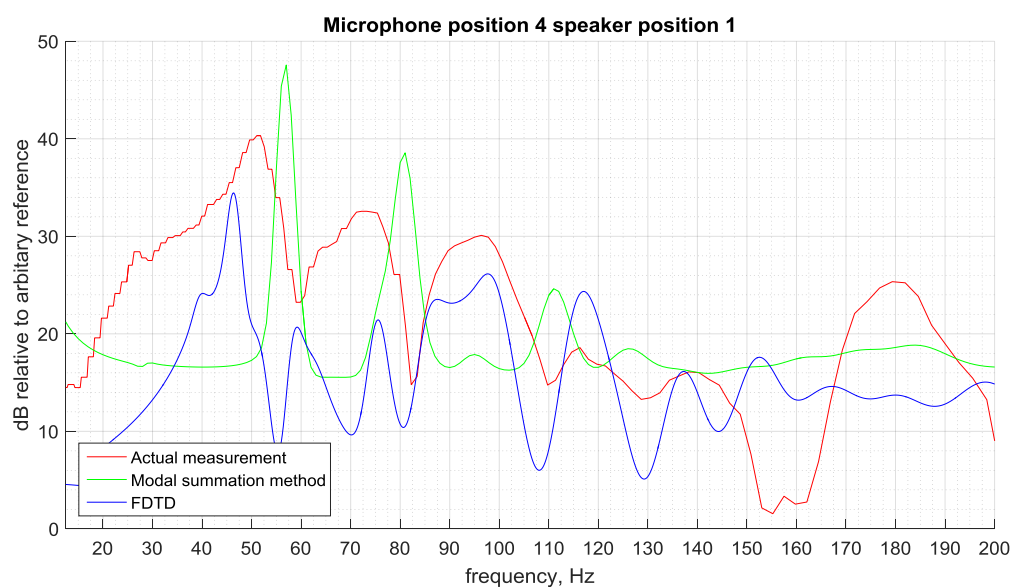


Figure 25

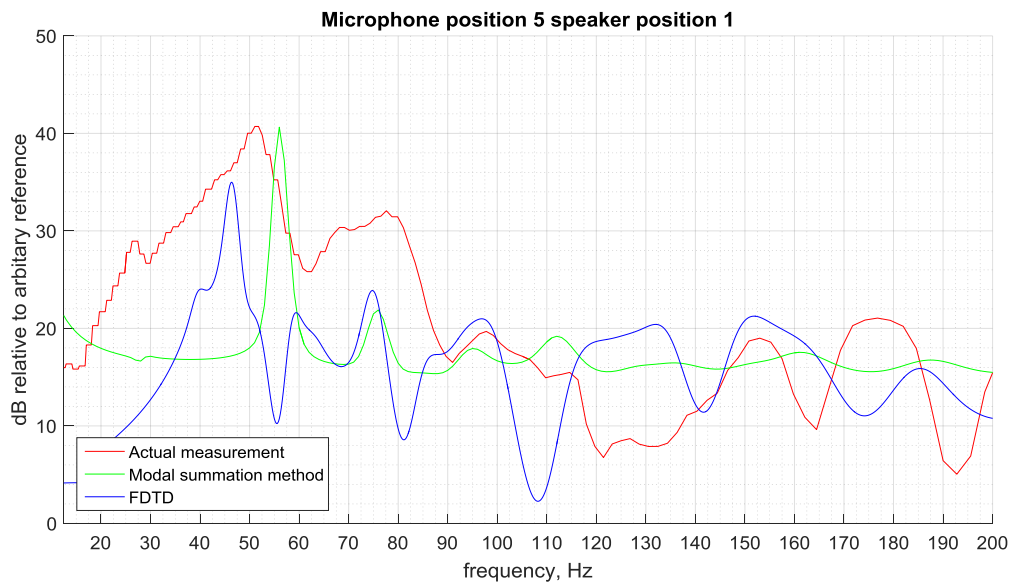


Figure 26

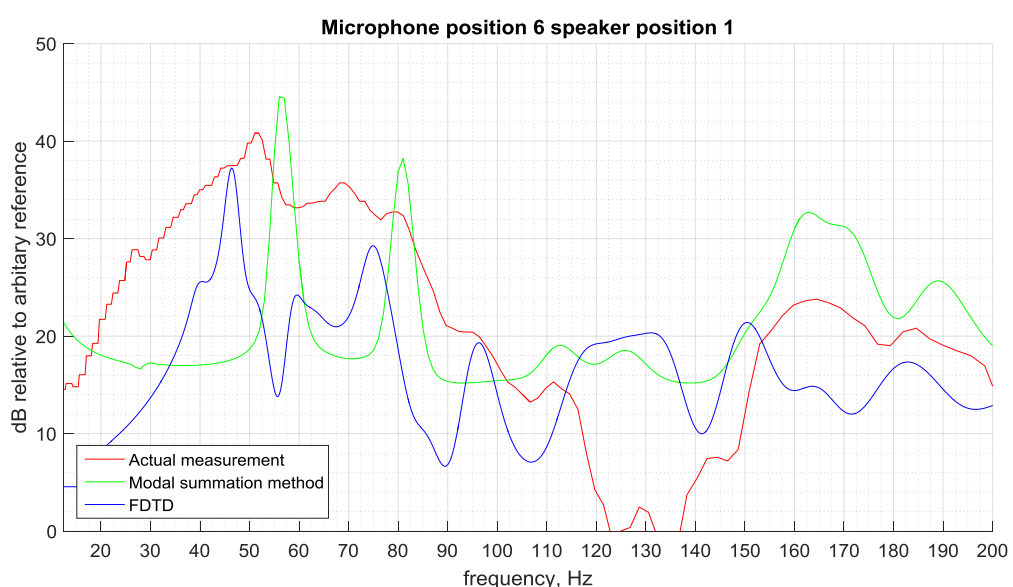


Figure 27

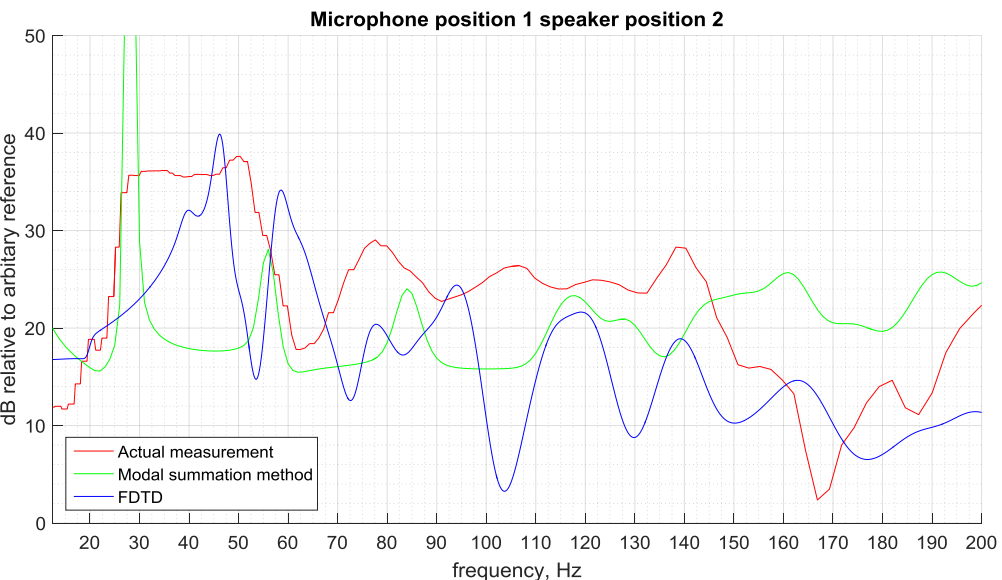


Figure 28

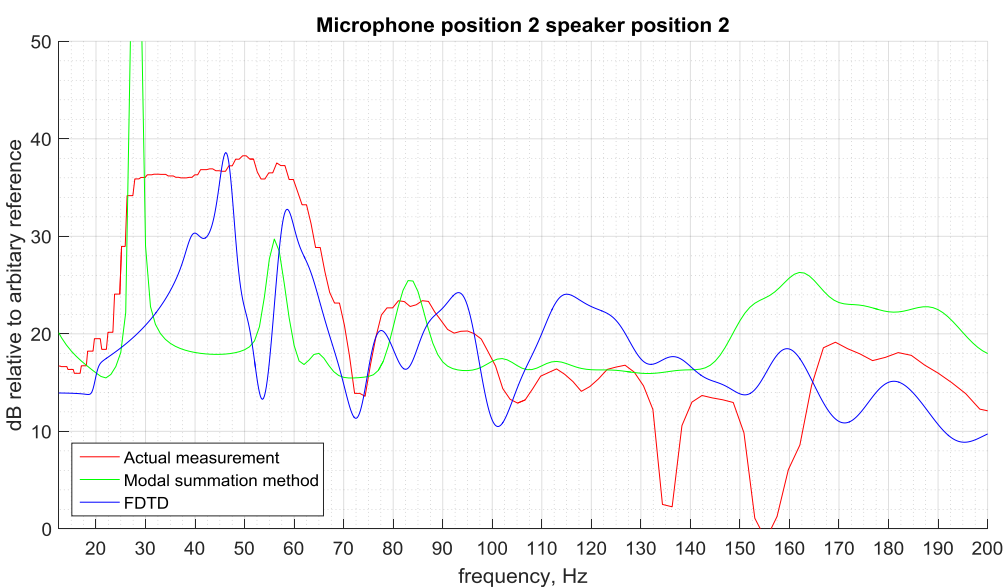


Figure 29

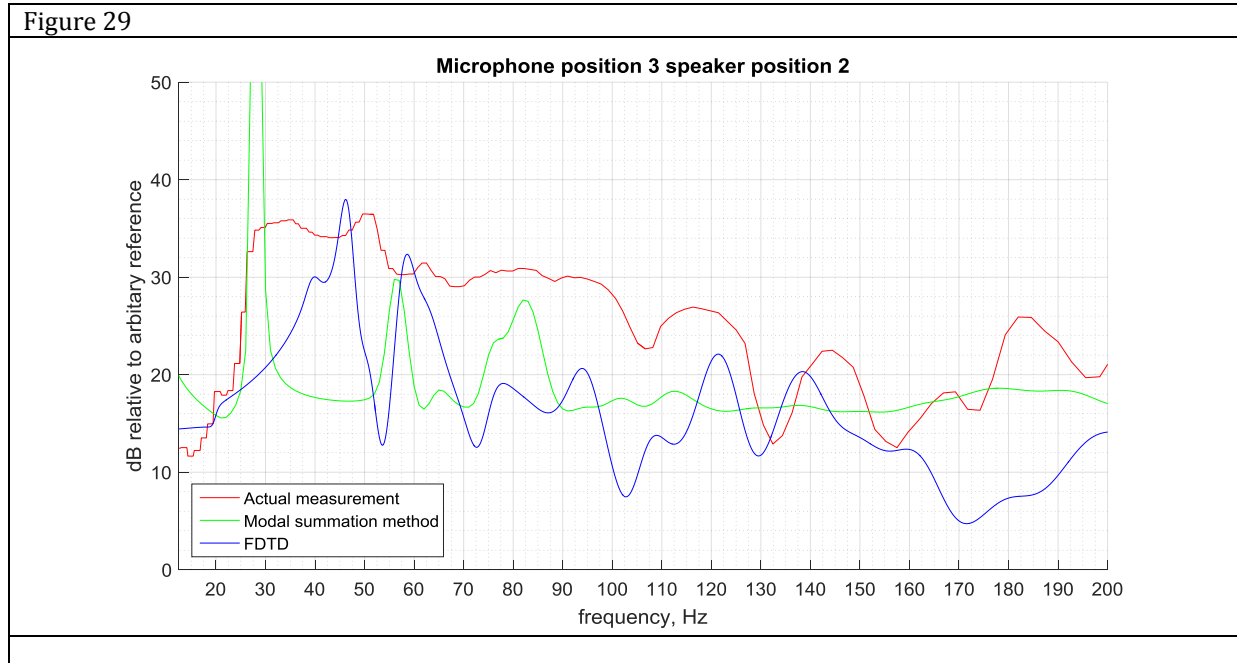


Figure 30

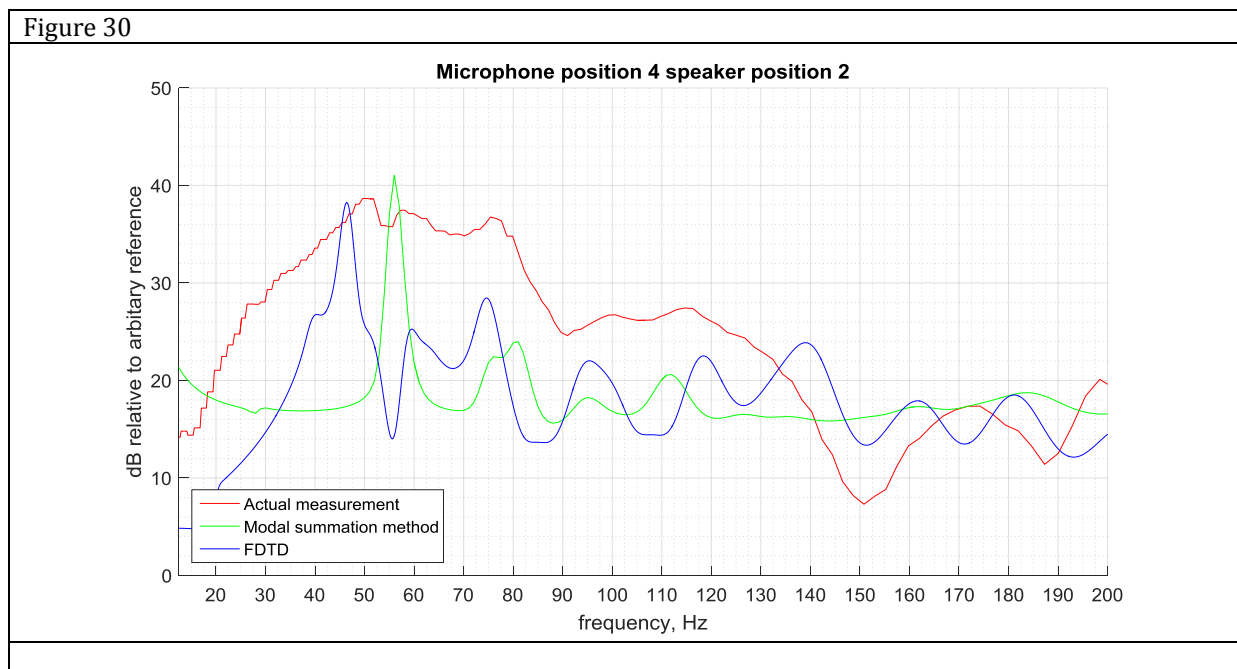


Figure 31

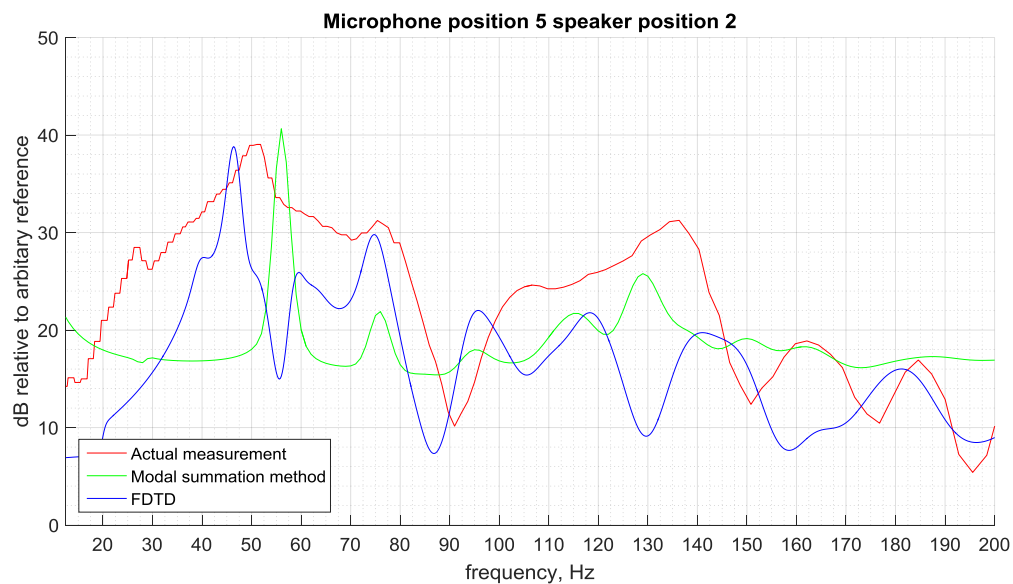


Figure 32

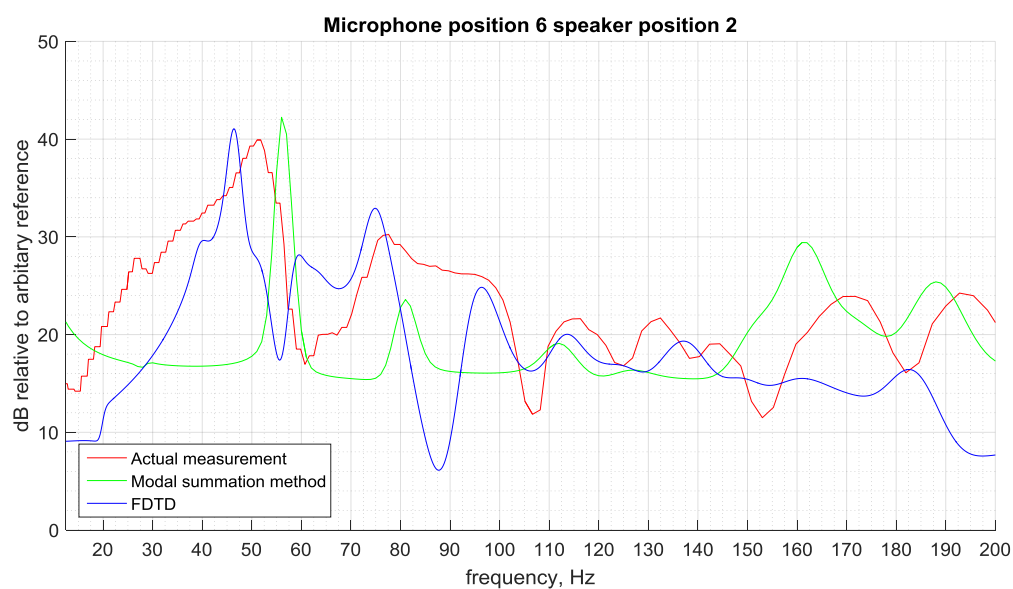


Figure 33

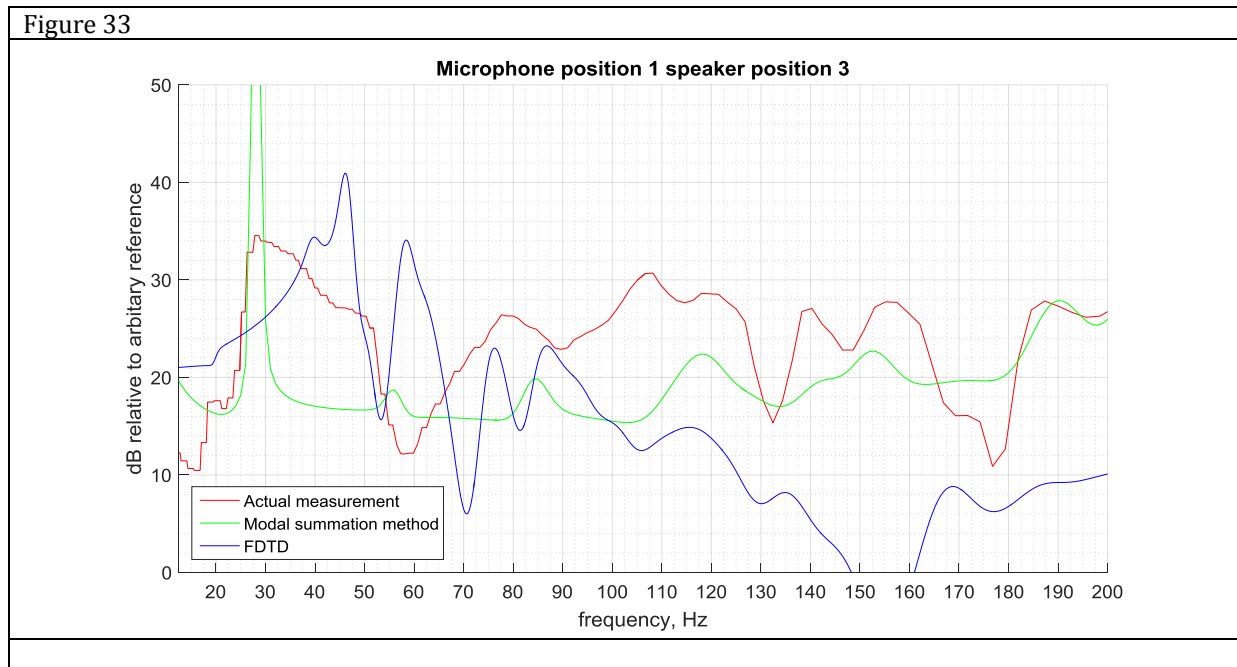


Figure 34

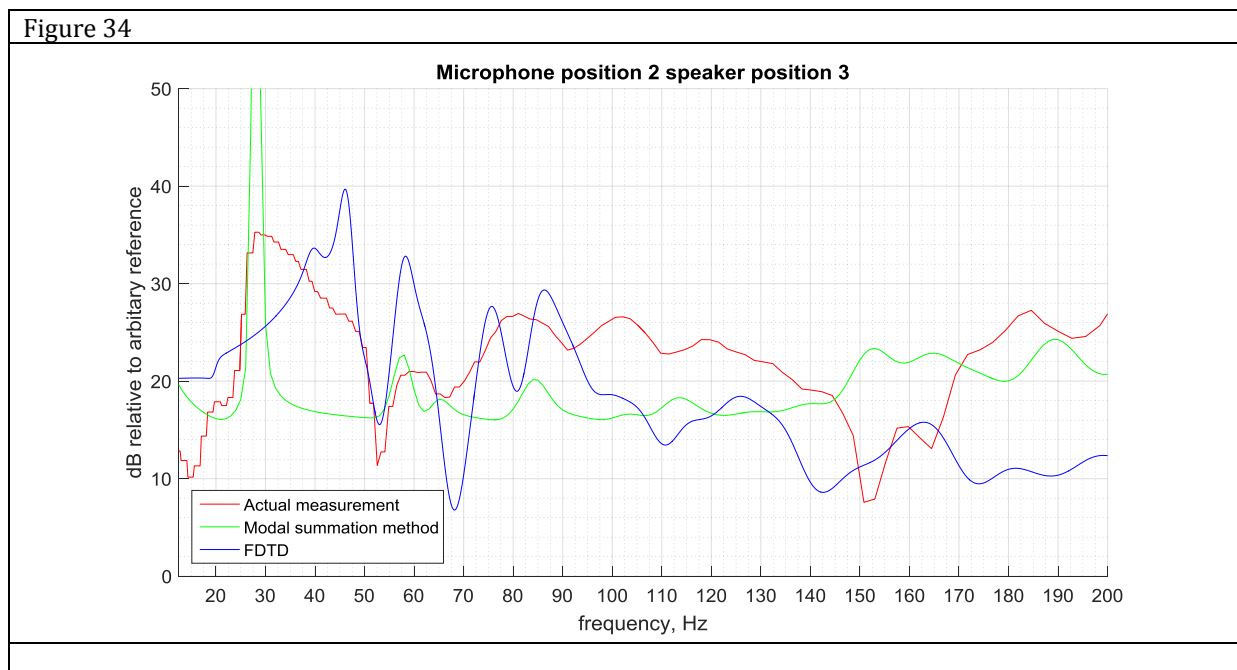


Figure 35

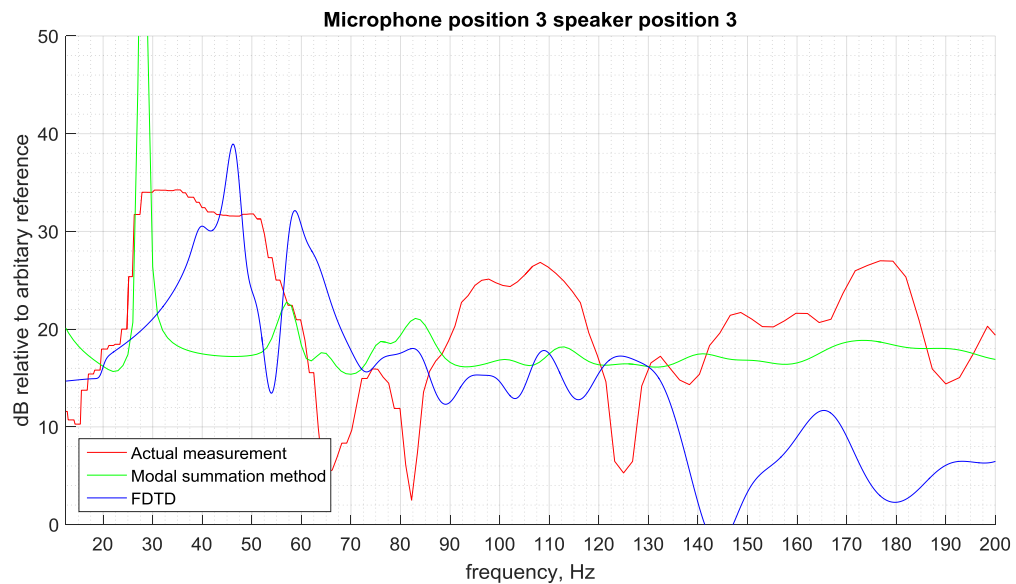


Figure 36

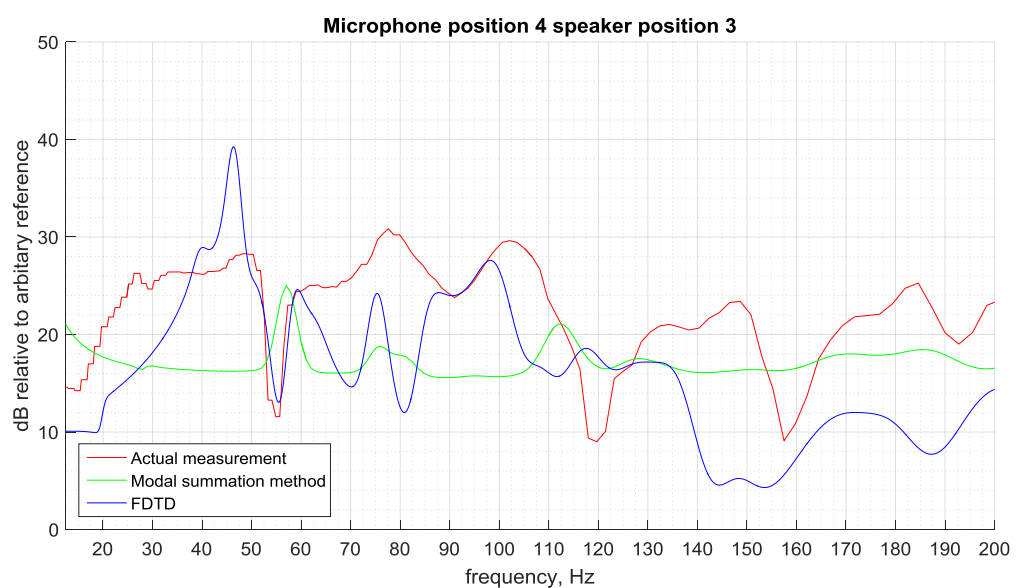


Figure 37

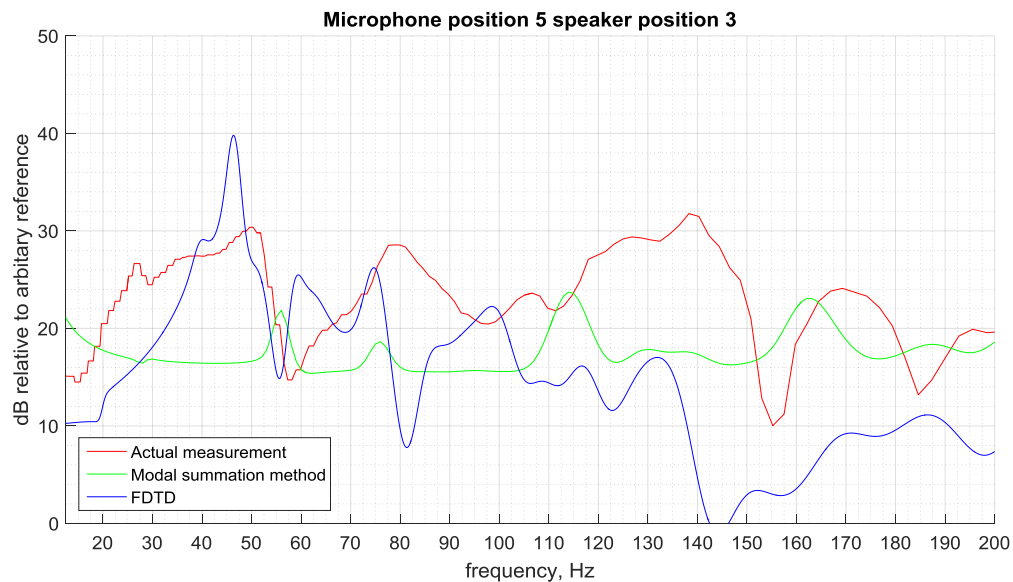


Figure 38

